



저작자표시-비영리-변경금지 2.0 대한민국

이용자는 아래의 조건을 따르는 경우에 한하여 자유롭게

- 이 저작물을 복제, 배포, 전송, 전시, 공연 및 방송할 수 있습니다.

다음과 같은 조건을 따라야 합니다:



저작자표시. 귀하는 원저작자를 표시하여야 합니다.



비영리. 귀하는 이 저작물을 영리 목적으로 이용할 수 없습니다.



변경금지. 귀하는 이 저작물을 개작, 변형 또는 가공할 수 없습니다.

- 귀하는, 이 저작물의 재이용이나 배포의 경우, 이 저작물에 적용된 이용허락조건을 명확하게 나타내어야 합니다.
- 저작권자로부터 별도의 허가를 받으면 이러한 조건들은 적용되지 않습니다.

저작권법에 따른 이용자의 권리는 위의 내용에 의하여 영향을 받지 않습니다.

이것은 [이용허락규약\(Legal Code\)](#)을 이해하기 쉽게 요약한 것입니다.

[Disclaimer](#)

Doctor of Philosophy

**MARINE APPLICATIONS OF FLAPPING FOILS/PLATES TO
THE STATIONKEEPING SYSTEM**

The Graduate School

of the University of Ulsan

Department of Naval Architecture and Ocean Engineering

Rupesh Kumar

MARINE APPLICATIONS OF FLAPPING FOILS/PLATES TO THE STATIONKEEPING SYSTEM

Supervisor: Shin Hyunkyoung

A Dissertation

Submitted to
the Graduate School of the University of Ulsan
In partial Fulfillment of the Requirements
for the Degree of

Doctor of Philosophy

by

Rupesh Kumar

Department of Naval Architecture and Ocean Engineering

University of Ulsan, Korea

December 2019

MARINE APPLICATIONS OF FLAPPING FOILS/PLATES TO THE STATIONKEEPING SYSTEM

This certifies that the dissertation of Rupesh Kumar is approved by



Committee Chairman: **Prof. Jung Rho-Taek**



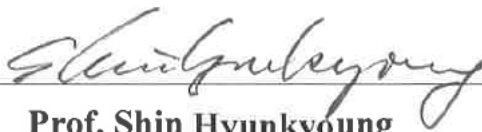
Committee Member: **Prof. Chung Kyung-Nam**



Committee Member: **Prof. Lee Hak-Gu**



Committee Member: **Prof. Lee Jin-Tae**



Committee Member: **Prof. Shin Hyunkyoung**

Department of Naval Architecture and Ocean Engineering

University of Ulsan, Korea

December 2019

Acknowledgements

I would like to express my sincere gratitude to Prof. Shin Hyunkyoung for his guidance and support throughout this work. Also, for providing me enough computational resources and software licenses for completing this work.

I would like to thank all my colleagues at the Widetank over the years, including Mr. Seo Beongcheon, Mr. Kim Junbae, Mr. Pham Thanh Dam, Miss. Ahn Hyeonjeong, Mr. Sim Woolim, Mr. Yu Youngjae, and Mr. Kim Jungtae for making work more fun and for their kind support.

I would like to thank Mr. Kim Dongju for providing me efficient experimental tools and technical support throughout this long process.

Finally, I would like to thank my family for supporting me in the difficult times. I certainly could not have done this without you behind me.

Abstract

Flapping motion is very common in nature. It's basically used for propulsion and maneuvering by birds, fish and many other species in air and water. Also, studies proved that the flapping motion has the capability of producing high instantaneous forces. In the ocean, when a hydrofoil placed horizontally close to the free surface, the hydrofoil can flap and generate thrust forces against the wave propagation using wave energy, famously called "wave devouring propulsion". However, exact estimation of forces generated by flapping remains a challenge for the researchers. Therefore, the uses of flapping are not so common in man-made structures. In this study, an elastic plate was used that was fixed at one end and attached to the leading edge of the hydrofoil or flat plate from another end. This setup minimizes the complexity of the flapping in water such as no phase lag between heave and pitch motions of the hydrofoil.

The passive flapping foil/plate experiments were carried out for various wave conditions in a wave flume at Widetank, UOU. The aim of the experiment was to use the flapping foil/plate to the stationkeeping system therefore, the model was flapping at a set location and the generated thrust forces were recorded using a load cell. Further, empirical formulas are derived for the thrust estimation of flapping foil and flapping plate using dimensional and regression analysis based on experimentally recorded data. The effects of elastic plate on thrust generation and the resultant thrust force generated by a group of flapping foils are also experimentally recorded and reported in this thesis.

The experimentally recorded data were validated with the fluid structure interaction (FSI) numerical simulation using ANSYS Workbench 19.2. It was a challenge to deal with 2-way FSI simulation with multiphase flow due to its complexity in defining geometries, interaction between a fluid and solid and requirements of computational resources. Results confirmed that the passive mode flapping wasn't effective for stationkeeping in short waves. Therefore, active flapping foil was modelled and thrust generated by it in short waves using numerical simulation were reported. Finally, the effects of azimuth angles of flapping foil on the thrust force in passive mode were reported in the thesis.

Contents

Contents	vi
List of Figures	ix
List of Tables	xiii
Nomenclature	xv
Chapter 1 Introduction	1
1.1 History of flapping foils	2
1.2 Applications of wave devouring propulsion	5
1.3 Why stationkeeping?	6
1.4 Background	6
Chapter 2 Passive Flapping Foil in Waves	9
2.1 Experiment set-up	9
2.1.1 Model preparation	12
2.1.2 Load cases	15
2.2 Experimental results	16
2.3 Effects of elastic plates on thrust	17
2.3.1 Length of elastic plate	18
2.3.2 Breadth of elastic plate	19
2.4 Conclusion	20
Chapter 3 Thrust Force Empirical Formula of a Flapping Foil	21
3.1 Dimensional analysis	21
3.2 Multiple regression analysis	23
3.3 Verification	27
3.4 Conclusion	28
Chapter 4 Combination of Foils	29
4.1 Two flapping foils in waves	29
4.2 Effects of azimuth angles	31
4.3 Two flapping plates	33
4.4 Multiple foils arranged in a circle	38
4.5 Fish cage with multiple foils and plates	40
4.6 Conclusion	44
Chapter 5 Passive Flapping Plate in Waves	45
5.1 Experiment setup	45
5.2 Thrust force measurements	47

5.3	Empirical formula for thrust force	48
5.4	Conclusion.....	52
Chapter 6	FSI Numerical Simulation Using CFD	55
6.1	Modelling	55
6.2	Computational mesh.....	56
6.2.1	Near wall treatment.....	56
6.2.2	Structured mesh	57
6.2.3	Load cases	58
6.2.4	Modal acoustic analysis	58
6.3	Solver settings	60
6.3.1	Boundary conditions	60
6.3.2	Fluent solver setup	61
6.3.3	System coupling setup	61
6.4	Results	62
6.4.1	Mesh convergence	62
6.4.2	Results comparison	64
6.5	Conclusion.....	65
Chapter 7	Active Flapping Foil	67
7.1	Forced oscillation	67
7.2	Fixed hydrofoil.....	68
7.3	Flapping in still water.....	70
7.4	Active mode results in short waves.....	71
7.5	Conclusion.....	72
Chapter 8	Validation of Results.....	73
8.1	Results comparison	73
8.2	Discussion	77
Chapter 9	Conclusion and Future Work.....	78
9.1	Conclusions	78
9.2	Future works.....	79
References	80
Appendix A	Foil Design	A-1
A.1	Lift and drag coefficients	A-1

List of Figures

Figure 1.1 - (a) Caudal fin with vertical flapping; (b) Flukes with horizontal flapping	1
Figure 1.2 – A drawing of Linden’s boat (Pearson’s Magazine, December 1898)	2
Figure 1.3 – A drawing from Schulze’s patent specification.....	2
Figure 1.4 – Wave powered boat model (Popular Science, 1935).....	3
Figure 1.5 – Fishing vessel with a bow hydrofoil (Terao and Isshiki, 1991)	3
Figure 1.6 – The propulsion mechanism of Suntory Mermaid II (Popular Science, 2008).....	4
Figure 1.7 – Fish propulsion mechanism (NTNU, 2017)	4
Figure 1.8 – Flapping foil (UOU)	7
Figure 1.9 – Ship propulsion in waves using passive flapping foil (UOU).....	7
Figure 2.1 – Experimental setup in a wave flume, UOU	9
Figure 2.2 – wave flume, UOU.....	10
Figure 2.3 – wave height and wavelength controller	11
Figure 2.4 – Experimental equipment.....	11
Figure 2.5 - Flapping foil	13
Figure 2.6 - Experiment plan	14
Figure 2.7 – Thrust measurement using load cell	16
Figure 2.8 – Experimental results	17
Figure 2.9 – Experiments to measure elastic modulus of elastic plate.	18
Figure 2.10 – Effects of the length of elastic plate on thrust force	19
Figure 2.11 – Effects of the breadth of elastic plate on thrust force	20
Figure 3.1 – Experimental results compared with the results obtained from the empirical formula.....	26
Figure 3.2 – Experimental results in widetank compared with the results obtained from the empirical formula.....	28
Figure 4.1 – Selection of elastic plates for the combined foil experiments.	29
Figure 4.2 – Combination of two highest thrusts (HT).....	30
Figure 4.3 – Combination of highest thrust (HT) and lowest thrust (LT).	30
Figure 4.4 – Comparison of case-1 and case-2	31
Figure 4.5 - Azimuth angles.....	32

Figure 4.6 – Effects of azimuth angles on thrust	33
Figure 4.7 – Combination of flapping flat plates	34
Figure 4.8 – Resultant thrusts due to combination of flapping flat plates	35
Figure 4.9 – Initial azimuth angles of flapping plates	35
Figure 4.10 – Azimuth angle control	36
Figure 4.11 – Effects of azimuth control on stationkeeping	37
Figure 4.12 – Multiple flapping foils arranged in a circle	38
Figure 4.13 – Two cases of stationkeeping model	39
Figure 4.14 – Results comparison of case-1 and case-2	40
Figure 4.15 – Experimental results in widetank compared with the results obtained from the empirical formula	41
Figure 4.16 – Experimental results in widetank compared with the results obtained from the empirical formula	41
Figure 4.17 – Experimental results in widetank compared with the results obtained from the empirical formula	43
Figure 4.18 – Experimental results in widetank compared with the results obtained from the empirical formula	43
Figure 5.1 – Experimental setup in wave flume	45
Figure 5.2 – Flapping flat plate	46
Figure 5.3 – Experimental results and comparison	48
Figure 5.4 – Experimental results compared with the results obtained from the empirical formula	52
Figure 6.1 – Flapping foil	55
Figure 6.2 – Geometry of fluid domain	56
Figure 6.3 – Mesh of fluid domain	57
Figure 6.4 – Mesh of solid domain	58
Figure 6.5 – Model of acoustic body	59
Figure 6.6 – Mesh of acoustic body	59
Figure 6.7 – Mesh of flapping body	60
Figure 6.8 – System coupling flow chart	62
Figure 6.9 – Force on fixed hydrofoil in x-direction	63
Figure 6.10 – Forces on fixed hydrofoil in z-direction	63
Figure 6.11 – Comparison of wave elevation and thrust forces	65
Figure 7.1 – Forced flapping profile	68
Figure 7.2 – Experimental setup to measure F_x for a fixed hydrofoil in short waves	69
Figure 7.3 – Comparison of wave profile and force in x-direction	69
Figure 7.4 – Thrust plot in still water using CFD (a) Flap-1; (b) Flap-2; (c) Flap-3; (d) Flap-4; (e) Flap-5	70

Figure 7.5 –Thrust plot in short waves (a) Passive flapping foil (Experiment); (b) Flap-1 (CFD); (c) Flap-2 (CFD); (d) Flap-3 (CFD); (e) Flap-4 (CFD); (f) Flap-5 (CFD)	71
Figure 8.1 – Estimation of mean thrust.....	74
Figure 8.2 – Comparison of results.....	76

List of Tables

Table 2.1 – Lengths of elastic plate	12
Table 2.2 – Breadths of elastic plate	12
Table 2.3 – Load cases	15
Table 2.4 – Wave heights (H)	15
Table 2.5 – Aspect ratio and area of the elastic plates	19
Table 3.1 – Parameters that influence the thrust force	21
Table 3.2 – Variables for multiple regression analysis	24
Table 3.3 – Results of regression analysis for the thrust generation of flapping foil	25
Table 3.4 – Load cases for widetank experiments.	27
Table 4.1 – Load cases for azimuth angle experiment.....	32
Table 4.2 – Load cases for combined foils experiments.....	34
Table 4.3 – Azimuth control of combined foils experiments.	37
Table 4.4 – Load cases for the experiments in widetank, UOU.	39
Table 4.5 – Azimuth control of combined foils experiments.	42
Table 5.1 – Load cases	47
Table 5.2 – Parameters that influence thrust force.	49
Table 5.3 – Results of regression analysis	51
Table 6.1 – Load cases for CFD simulation	58
Table 6.2 – Boundary conditions of fluid domain	60
Table 6.3 – solver setup	61
Table 6.4 – Mesh resolution.....	63
Table 7.1 – Mesh resolution.....	67
Table 7.2 – Wave specification.....	69
Table 8.1 – Load cases for CFD simulation	73
Table 8.2 – Estimation of thrust coefficient from empirical formula	75
Table 8.3 – Thrust coefficient of experimental and numerical methods	76

Nomenclature

FSI: Fluid Structure Interaction

CFD: Computational Fluid Dynamics

CSM: Computational Structural Mechanics

RANS: Reynolds Averaged Navier Stokes Simulation

VOF: Volume of Fluid

CV: Control Volume

SIMPLE: Semi Implicit Method

HRIC: High Resolution Interface Capture

HDPE: High Density Polyethylene

HT: Highest Thrust

LT: Lowest Thrust

UOU: University of Ulsan

Ct: Thrust coefficient

Ar: Aspect ratio

Ws: Wave slope

Fn: Froude number

Rn: Reynolds number

Ep: Elastic plate number

Ad: Added mass number

L: Length of elastic plate

B: Breadth of elastic plate

S: Span of hydrofoil

C: Chord of hydrofoil

t: thickness

Lw: Wavelength

Hw: Wave height

RPM: Rotation per minute

T: Time period

ω : Wave frequency

λ : Wavelength

A: Wave amplitude

L1: $L/C = 1.125$

L2: $L/C = 0.750$

L3: $L/C = 0.375$

B1: $B/S = 1.0$

B2: $B/S = 0.5$

B3: $B/S = 0.2$

Chapter 1 Introduction

In nature, birds, fish, and insects maneuver using their wings or tails. That is, maneuvering forces are generated by the flapping motion of their foil-shaped wings, fins or tails, which produce thrust by means of a direct conversion from fluid flow to propulsive energy. In air, birds flap its wings attached from both sides to the body called “side flapping”. In water, majority of fishes have vertically aligned caudal fins, flap left to right called “vertical flapping” however, whales and dolphins have horizontally aligned flukes and its up and down motion called “horizontal flapping”.

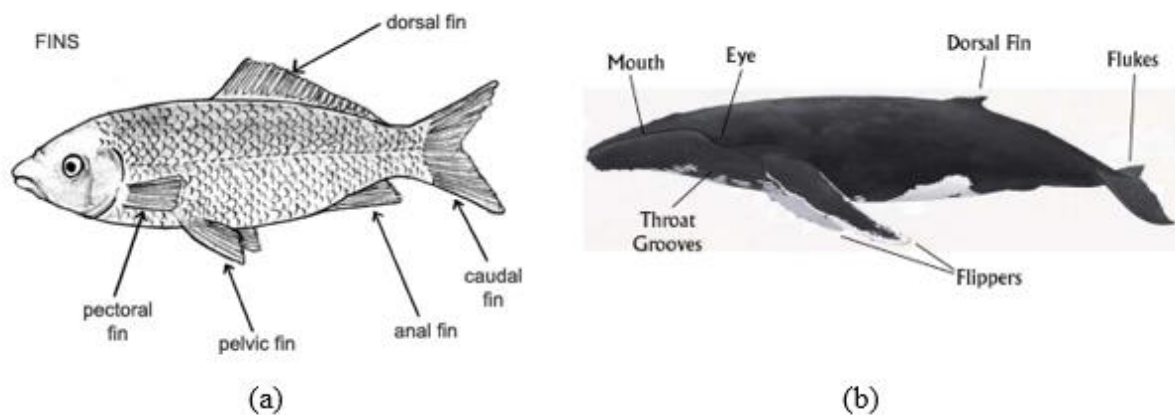


Figure 1.1 - (a) Caudal fin with vertical flapping; (b) Flukes with horizontal flapping

[source: Google]

Flapping motion requires a continuous source of excitation energy for producing instantaneous forces. Therefore, flapping of wings, tails and fins are active in nature. Passive flapping is possible when energy was extracted from renewable sources such as sea surface waves, the most commonly found energy sources in the world.

1.1 History of flapping foils

The thrust generating ability of flapping foil has inspired numerous researchers to improve the propulsive and maneuvering abilities of floating structures in water. In 1895, Hermann Linden [1] in Naples, Italy, built a 13 ft long boat as shown in Figure 1.2, which moved against the waves at three to four miles per hour, powered purely by the thrust generated from two underwater steel plates using wave energy.

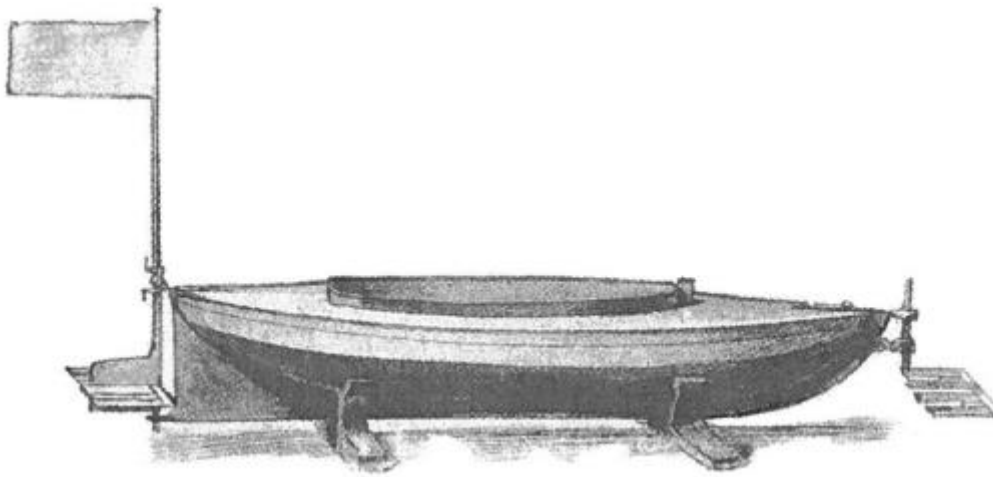


Figure 1.2 – A drawing of Linden’s boat (Pearson’s Magazine, December 1898)

In 1911, Otto Schulze [2] of Brooklyn, New York, designed a boat with fins where fins can generate electricity using wave energy and the generated electricity can be used for driving the propeller.

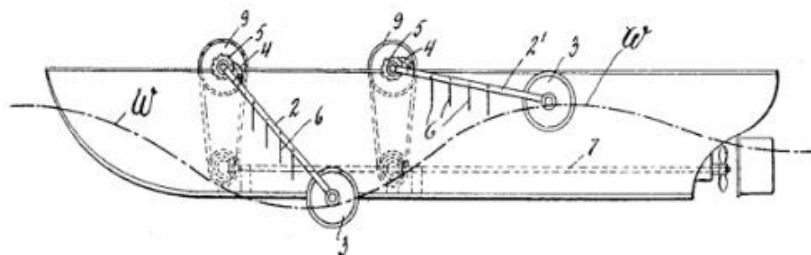


Figure 1.3 – A drawing from Schulze’s patent specification

In 1935, Popular Science [3] claims a wave powered boat with two fins in the bow and one fin in the stern. This 18-inch model could move at 5 miles per hour speed, however, the size of fins was relatively large compared to the hull, as shown in Figure 1.4.

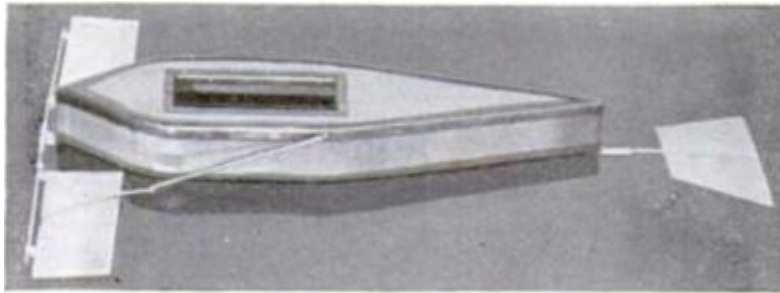


Figure 1.4 – Wave powered boat model (Popular Science, 1935)

In 1950, Popular Science [4] published another wave-powered boat designed by John S. McCubbin of Victoria, Australia. In 1966, Gause [5] filed his first patent for a wave powered boat, he attached three flexible fins to a 34 ft boat and attained a maximum speed of 5 mph using energy of the waves. In 1991, Hiroshi Isshiki and Yutaka Terao [6] of Japan, carried out full scale tests on 15.7 m long fishing vessel with a bow hydrofoil as shown in Figure 1.5. The hydrofoil area was 7.4 % of ship's waterplane area which increased the boat speed in waves also, reduced pitching motion and bow slamming.



Figure 1.5 – Fishing vessel with a bow hydrofoil (Terao and Isshiki, 1991)

In 2008, Yutaka Terao [7] designed a wave powered catamaran Suntory Mermaid II as shown in Figure 1.6, which sailed from Honolulu, Hawaii to the Kii Channel, Japan in 110 days. The journey is to date the longest known voyage by a wave-powered boat.

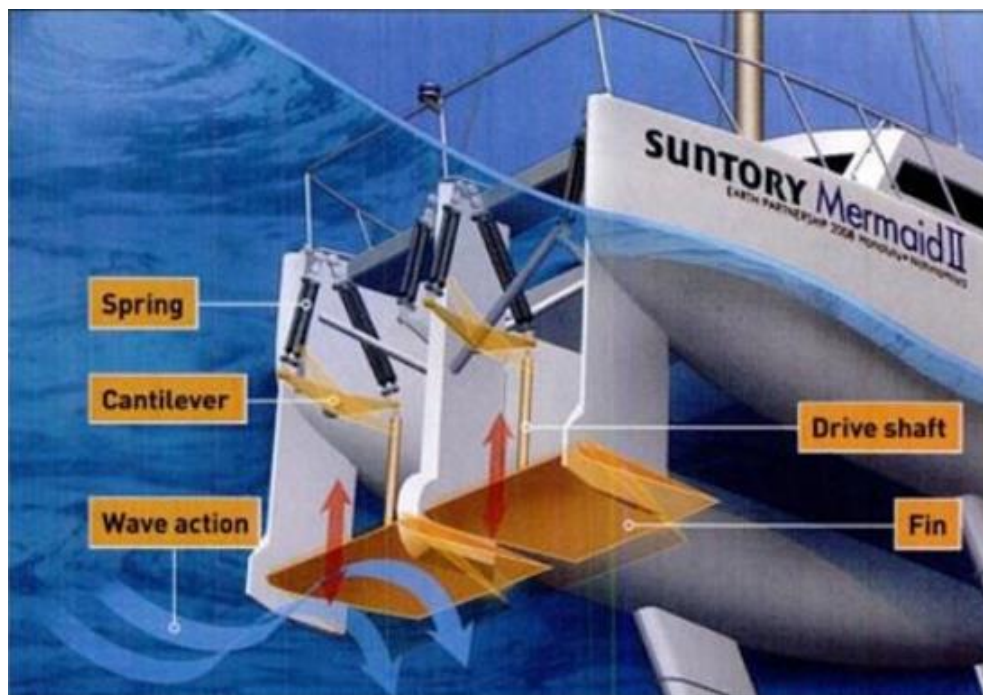


Figure 1.6 – The propulsion mechanism of Suntory Mermaid II (Popular Science, 2008)

In 2017, John Martin Godo [8] of Norway, presented a new propulsion system using flapping foils as shown in Figure 1.7, he used two flapping foils that flapped together in and out of phase over angles of 180° , which could generate lift and forward thrust with better efficiency compared to screw propellers.

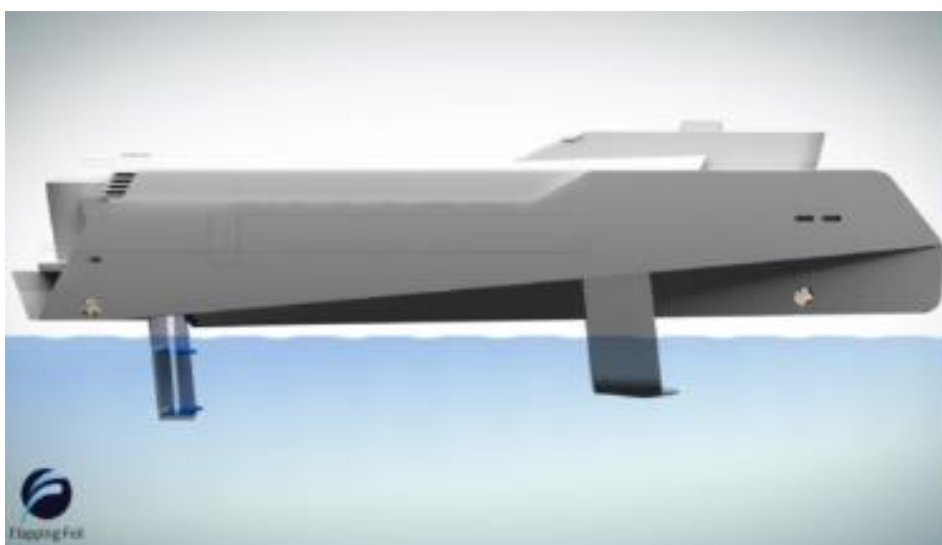


Figure 1.7 – Fish propulsion mechanism (NTNU, 2017)

1.2 Applications of wave devouring propulsion

A model ship could move against incoming waves with the aid of flapping foils alone and the ship speed was dependent on the wave conditions, a phenomenon known as “wave devouring propulsion.” It was also found that the flapping foil propulsion system has higher efficiency, lower noise, better manoeuvrability and control systems [9,10]. Subsequently, the application of flapping foil as an auxiliary propulsor near the free surface have been studied [11], [12]. Read [13] and Hover [14] reported on the forces on flapping foils for propulsion and maneuvering, and the effects of the attack angle on flapping foil propulsion, respectively.

In 1958, Ulysses [15] experimented with a boat that had four fixed fins and found that the fins were capable of not only increasing the thrust but also reducing pitch boat motion. These foils are referred to as “anti-pitching fins.” Subsequently, researchers changed the foil location to obtain other advantages, such as anti-rolling [16]. Afterwards, many innovative ideas were presented on flapping flexible foils [17]. Studies on the chord-wise flexibility of a flapping foil were presented [18]. They found that the efficiency of the foil was increased due to the chord-wise flexibility of the foil compared to rigid foils. Subsequently, researchers had experimented with span-wise flexibility [19]. It was found that the span-wise flexibility could improve the propulsive efficiency by adjusting the motions and flexibility parameters. Recently, Liu [20] presented a research study on the flapping foil with a plate connected to the trailing edge of the foil. He used a spring in the tail to make it flexible and found that an oscillating plate connected to the trailing edge of the flapping foil could enhance the performance of the system.

Despite extensive studies on the flapping foil dynamics, the experimental measurements of the thrust force without forward motion has drawn relatively less scientific interest. Most of the researchers have studied the heave and pitch motion of the foil against incoming free stream [21], [22] or the foil itself moving in steady forward motion [20], [23], [24]. Also, fewer studies have been carried out on the flapping foil extracting energy from the free surface waves. Silva [25] numerically studied the performance of a two-dimensional rigid foil in gravity waves. The investigated results explained that when some key parameters are correctly maintained, the flapping foil could increase its performance in waves. Therefore, from the previous literatures it can be summarized that a flexible foil flapping near the free surface could be more efficient

for the generation of thrust forces. However, the measurement of flexibility has not drawn much interests of the researchers so far. Also, when we think of stationkeeping of a floater in waves using flapping foils, the measurement of thrust forces generated by a flapping foil in waves without any forward velocity becomes important.

1.3 Why stationkeeping?

The offshore industries are moving from shallow to deeper water. The conventional methods for the stationkeeping of deep-water floaters became more complex and expensive. Therefore, stationkeeping using flapping foils could provide the following advantages;

- It can be installed regardless of water depth.
- It has no use of mooring lines.
- It's easy to relocate.
- It uses energy from the waves to operate.
- Cost-effective.

1.4 Background

When a hydrofoil was placed horizontally in waves, it could flap up and down due to vertical component of the wave orbital velocity and could generate thrust forces against the wave propagation. For flapping within the stall limit, a restoring force should be imposed on the flapping model, hinge and spring were famous among the researchers in the past, however, those models could only flap in pitch motion about the support point. In my experiments, an elastic plate was attached to the leading edge of hydrofoil for restoring, so that, hydrofoil could flap smoothly under the stall limit in heave and pitch motions as shown in Figure 1.8, also, the elastic plate kept heave and pitch motions of hydrofoil in-phase to minimize the complexity in flapping. Hydrofoil and elastic plate were made of acrylic glass and HDPE respectively to maintain the neutral buoyancy in water.

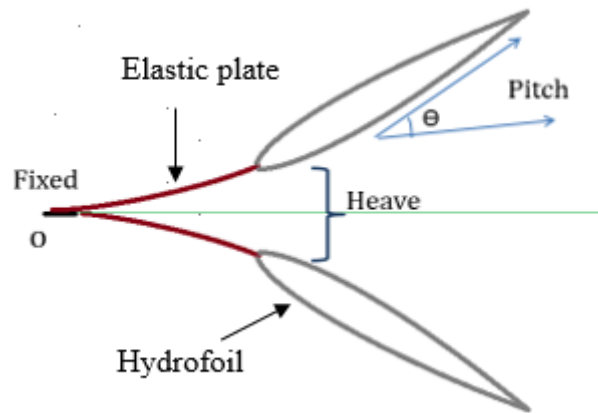


Figure 1.8 – Flapping foil (UOU)

First, the flapping foil was attached to the bow of a 1.5 m long container ship (KCS) model without propeller as shown in the Figure 1.9 and experiments were carried out in the wave flume. Results confirmed the forward motion of the ship in waves against the wave propagation.

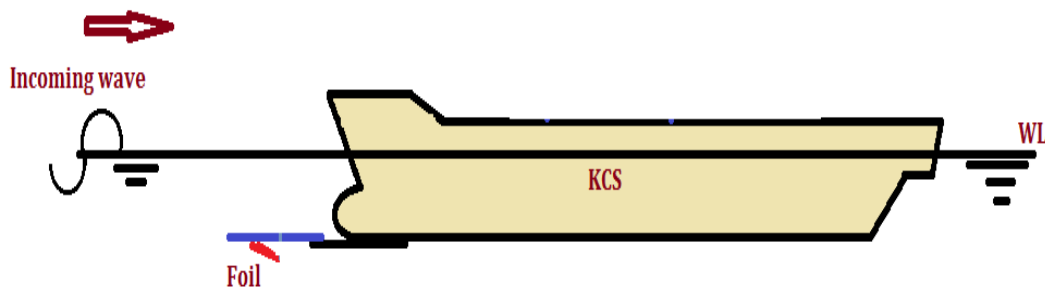


Figure 1.9 – Ship propulsion in waves using passive flapping foil (UOU)

Since, aim was to study the application of flapping foils to the stationkeeping of a floater in waves, experiments have been carried out with a hydrofoil flapping at a set location in various wave conditions. Thrust forces generated by a flapping foil was recorded using a loadcell in time-domain. Further, based on experimentally recorded data, an empirical formula for thrust estimation of a flapping foil in waves was developed using multiple regression analysis. The study was repeated for the flapping flat plate as well due to its simple geometry and ability to generate thrust forces. The effects of elasticity of the plates and azimuth angles of the flapping

foil were also reported. Furthermore, the experimental results were validated by the FSI-CFD simulation using numerical tool ANSYS Workbench 19.2, active and passive modes of flapping foil were simulated. For the past few years, due to technical advancements in the field of computational fluid dynamics (CFD), the numerical analysis has become more realistic to be performed in a reasonable time frame. Also, CFD can be coupled with the computational structural mechanics (CSM) to simulate several multi-physics problems such as fluid-structure interaction (FSI). In recent years, FSI simulations are conducted to evaluate the environmental loads and dynamic response of the offshore structures [26]–[28] and many aerodynamic [29], [30] and biomedical applications [31], [32].

Finally, a thrust force comparison of experimental data, numerical simulation and empirical formula were compared and validated.

Chapter 2 Passive Flapping Foil in Waves

In this chapter, we carried out experiments with a rigid foil connected to a flexible plate to its leading edge in surface gravity waves and the thrust forces generated by the flapping motion of the foil were recorded. We also observed experimentally that a minor change in the elastic plate attached to the leading edge of the foil can have a significant effect on the thrust generation of the flapping foil.

2.1 Experiment set-up

The flapping foil experiments were carried out in a wave flume in the Ocean Engineering Lab, University of Ulsan. The flume was 35 m long, 0.5 m wide, and 0.6 m deep. A wave-maker was located at one end of the tank to generate the desired waves. At the other end of the tank, a wave absorbing beach was used to dissipate the wave energy and reduce wave reflection. The water depth and submergence of the foil were, respectively, equal to 0.4 m and 0.05 m and were unchanged during the experiments.

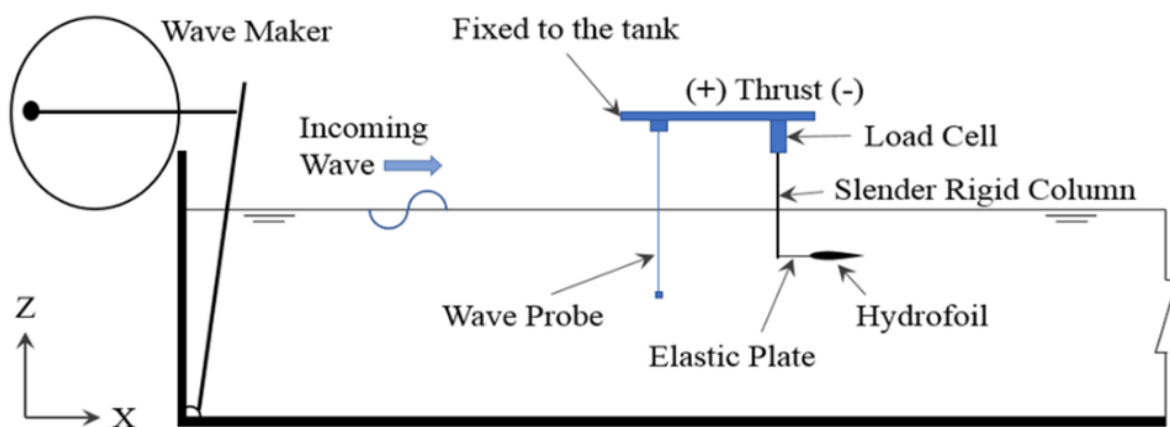


Figure 2.1 – Experimental setup in a wave flume, UOU

A wave probe was mounted on the fixed frame of a tank, which was positioned 3 m away from the wave paddle. The wave probe was able to measure the water level fluctuations to the nearest 0.5 mm. The diameter of the probe wire was 0.3 cm and its placement in the water before the flapping foil did not cause any significant modification to the wave field. A load cell was mounted on the fixed frame of the tank, which was positioned 0.2 m from the wave probe. The load cell was able to measure the thrust forces in the x-direction of the wave flume as shown in Fig 2.1 [33]. The maximum capacity of the load cell was 10 N and was changed to 0.2 N to increase the accuracy of the measurements. The load cell was set to produce 100 observations per second. In general, the load cell was used to record the thrust force of the flapping foil, whereby the flapping foil was attached to the load cell through a slender rigid column. Therefore, a thrust force generated by a flapping foil was experienced by the slender rigid column, which transferred the thrust force to the load cell to record it. Thrust forces measured along the direction opposite to the incident wave were recorded as positive, and the forces measured along the direction of the wave, as negative. The experimental setup is displayed in Fig. 2.1.



Figure 2.2 – wave flume, UOU



RPM	
Maximum	60 RPM
Minimum	05 RPM



Stroke	
Maximum	210 mm
Minimum	100 mm

Figure 2.3 – wave height and wavelength controller



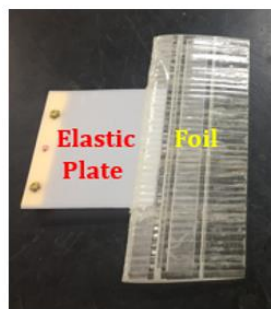
- Edinburgh Designs Ltd
- 8Channel system with probes
- Range : ± 0.25 m
- Power source : AC 220V
- Wave calibration

**Load Cell**

Capacity = 1kg

Calibrated Capacity = 100g

Material = Aluminum Alloy

**Neutrally Buoyant Foil**

Section: NACA0015
 Material: Acrylic Glass
 Chord: 8 cm
 Foil Span: 20 cm
 Foil Weight: 125 g

Elastic Plate

Material: PE
 Density: 0.93 g/cm³
 Thickness: 0.1 cm

Figure 2.4 – Experimental equipment

2.1.1 Model preparation

The foil used for all the experiments was rectangular with a constant NACA0015 section, a chord of 8 cm, and a span of 20 cm. It was rigid, neutrally buoyant, and constructed of acrylic. The elastic plate was also rectangular with a constant thickness of 0.1 cm and made of polyethylene. The flat plate was attached to the leading edge of the rigid foil, as displayed in Figure 2.5. The dimensions of the hydrofoil remained constant throughout the experiments. However, the dimensions of the elastic plate varied as shown in the Table 2.1 and Table 2.2. Where L represents the length of elastic plates, B represents the breadth of elastic plates, C and S represent chord and span of the hydrofoil respectively. The plan used for carrying out experiments is shown in detail in Figure 2.6 where a rigid hydrofoil was experimented with three different lengths of elastic plates and each length of elastic plates attached with the hydrofoil was experimented with the three different breadths of the elastic plates. Therefore, total nine models were prepared for the experiments and each model consists of the same hydrofoil.

Table 2.1 – Lengths of elastic plate

Length	L1	L2	L3
L/C	1.125	0.750	0.375

Table 2.2 – Breadths of elastic plate

Breadth	B1	B2	B3
B/S	1.0	0.5	0.2

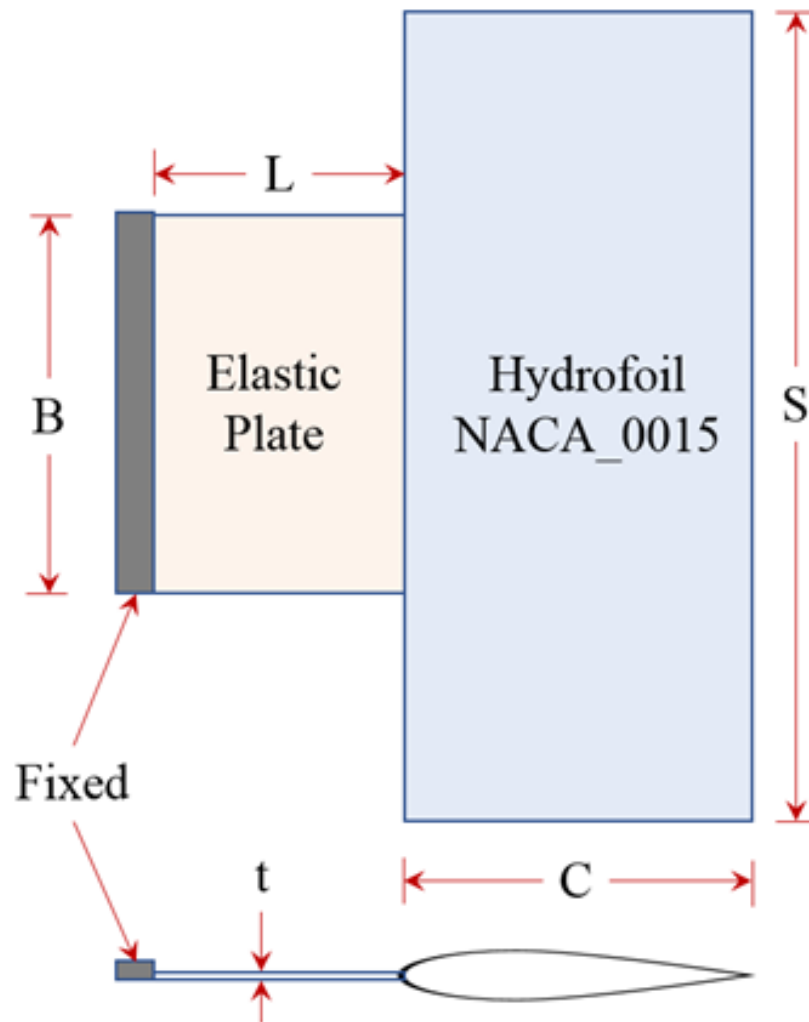


Figure 2.5 - Flapping foil

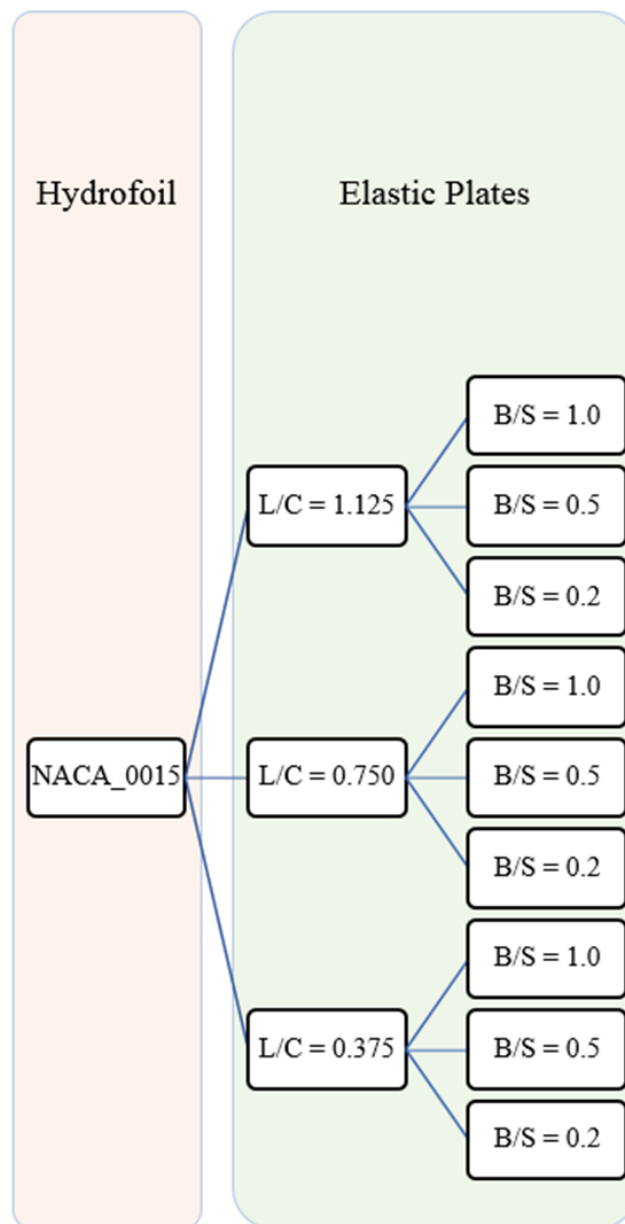


Figure 2.6 - Experiment plan

2.1.2 Load cases

Flapping foil experiments were performed for the twenty-four wave conditions for each set of the models, as shown in the experimental plan of Figure 2.6. Table 2.3 shows eight load cases for wavelengths (L_w) in the range of 0.25 m to 3.69 m. These wavelengths are repeated for three wave heights (H), as shown in Table 2.4. Therefore, 24 load case experiments were carried out in total for each set of the models.

Table 2.3 – Load cases

Serial Number	RPM	Period (s)	Status	K	ω (rad/s)	L_w (m)
1	10	2.0	Finite	1.7	3.13	3.69
2	15	1.4	Finite	2.7	4.63	2.30
3	20	1.0	Finite	4.2	6.22	1.49
4	25	0.8	Finite	6.2	7.75	1.01
5	30	0.7	Deep	8.7	9.24	0.72
6	35	0.6	Deep	12.0	10.86	0.52
7	40	0.5	Deep	15.5	12.32	0.41
8	50	0.4	Deep	25.2	15.71	0.25

Table 2.4 – Wave heights (H)

Serial Number	H(mm)
1	10
2	20
3	30

2.2 Experimental results

Figure 2.7 shows the thrust forces in time domain generated by a flapping foil during experiments. The positive and negative thrusts were obtained for each stroke of the flapping motion of foil and mean value was observed as the thrust force for the regression analysis.

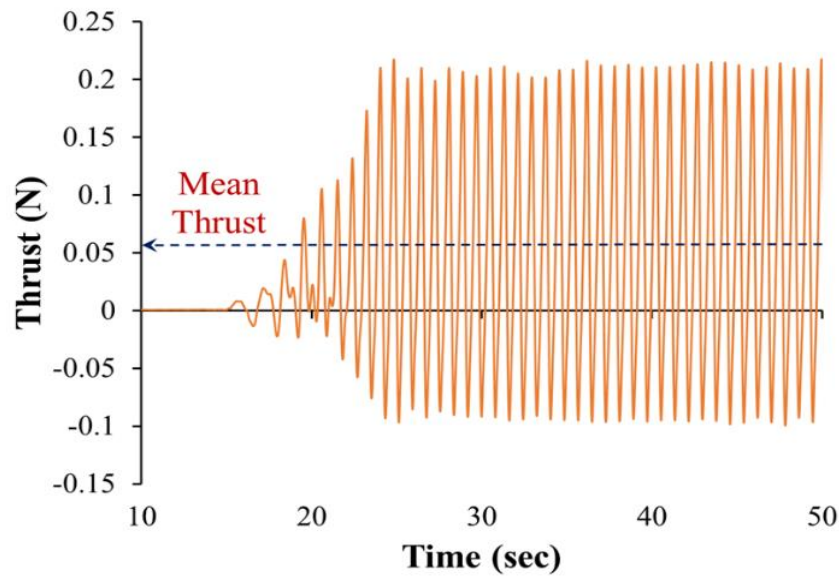


Figure 2.7 – Thrust measurement using load cell

Figure 2.8 presents the experimental results of the flapping foil. Additionally, a comparison of the thrust generation of a flapping foil for three different wave heights (10 mm, 20 mm and 30 mm) is displayed. Table 2.1 and Table 2.2 define L1, L2, L3 and B1, B2, B3 respectively.

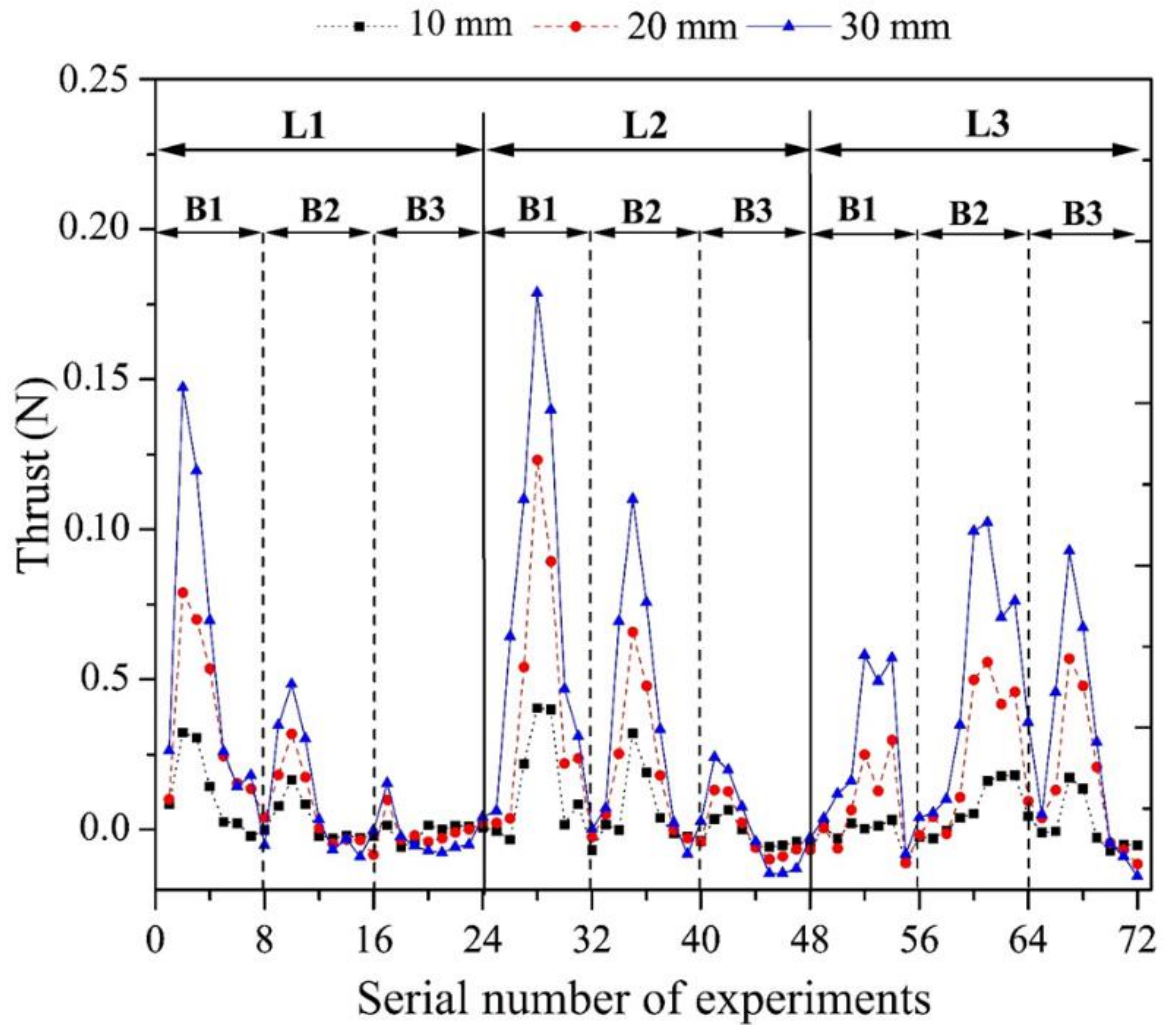


Figure 2.8 – Experimental results

2.3 Effects of elastic plates on thrust

This section includes the effects of the length and breadth of elastic plates on the thrust generation of flapping foil in waves. Figure 2.9 shows the experiments carried out to measure the elastic modulus of the plate.

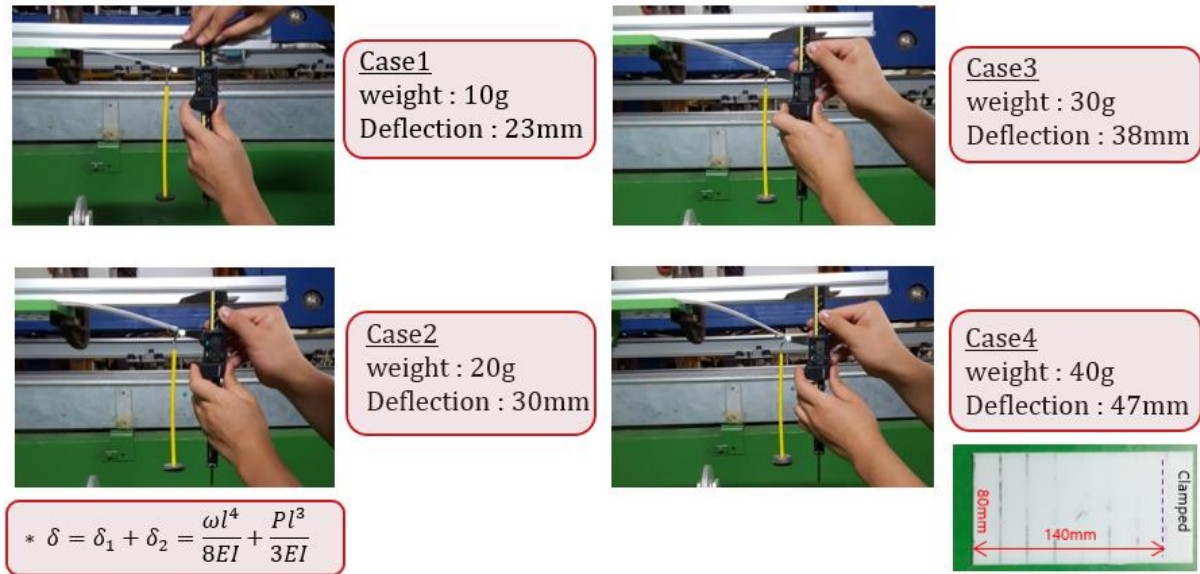


Figure 2.9 – Experiments to measure elastic modulus of elastic plate.

2.3.1 Length of elastic plate

The effectiveness of the elastic plate was largely dependent on the aspect ratio (L/B) and the area of the elastic plates (A_{EP}) as shown in Table 2.5. The lengths (L) of the elastic plate have significant effects on the thrust estimation of the flapping foil. As shown in Figure 2.10, when the breadth is fixed to $B1$, the foil with larger length ‘ $L1$ ’ could displace more from its original position and would have larger oscillating period. Thus, it is more suitable for long waves. On the other hand, when the length of the elastic plate is smaller, the foil could have a smaller deflection and oscillating period thus, is suitable for the short waves. Also, the low aspect ratio with bigger area generates bigger thrust therefore, in case of $B1$, $L2$ generates bigger thrust compared to $L1$ and $L3$. The effects of aspect ratio could be observed when the breadth of elastic plate was fixed to $B2$ as well. In case of $B3$, $L1$ and $L2$ show peculiar trends because $B3$ was the smallest breadth and the aspect ratios were very high as 2.25 and 1.50 respectively. It means, elastic plates were very much flexible and only suitable for very long waves.

Table 2.5 – Aspect ratio and area of the elastic plates

Length	Breadth	L/B	$A_{EP} \text{ (cm}^2\text{)}$
L1	B1	0.45	180
	B2	0.90	90
	B3	2.25	36
L2	B1	0.30	120
	B2	0.60	60
	B3	1.50	24
L3	B1	0.15	60
	B2	0.30	30
	B3	0.75	12

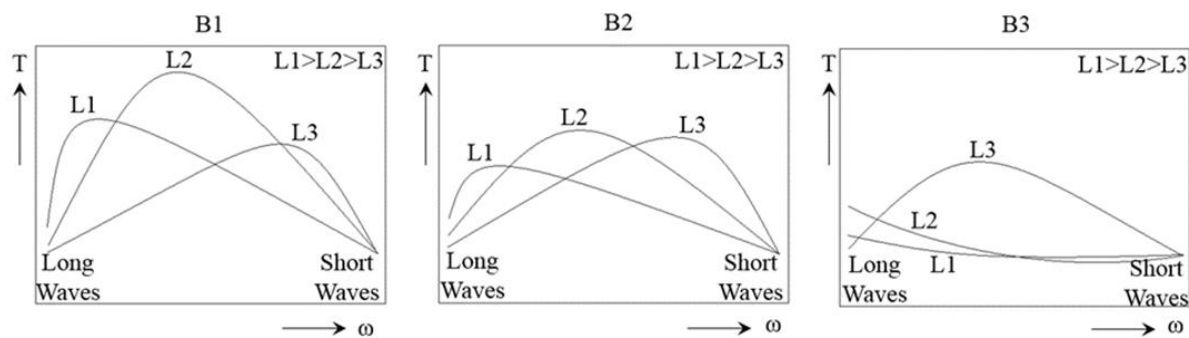


Figure 2.10 – Effects of the length of elastic plate on thrust force

2.3.2 Breadth of elastic plate

The breadth (B) of the elastic plate also has a significant effect on the thrust estimation of the flapping foil. When the breadth is larger, the foil could not displace more from its neutral position owing to an increase in the rigidity of the elastic plate and oscillate with the shorter time period. Thus, it was more suitable for middle-sized and short waves, as shown in Figure 2.11. On the other hand, when the breadth of the elastic plate was smaller, it was more suitable for long waves due to decreased rigidity of the elastic plates.

In general, the bigger area of the elastic plate generates bigger thrust as shown in L1 and L2 case of Figure 2.11. Where B1 is bigger than B2 and B3 thus B1 generates bigger thrust followed by B2 and B3. However, in case of L3, B2 and B3 generates bigger thrust than B1 due to very low aspect ratio ($L/B = 0.15$).

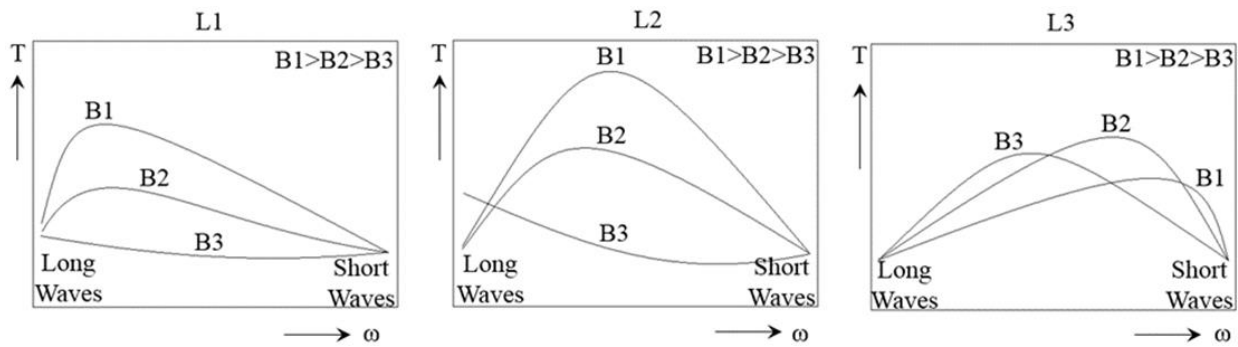


Figure 2.11 – Effects of the breadth of elastic plate on thrust force

Therefore, it can be concluded that the aspect ratio of the elastic plate ($E = 1$ GPa, $t = 0.1$ cm) should be ($0.2 < L/B < 1.0$) for the effective thrust generation of flapping foil in regular waves.

2.4 Conclusion

The experimental results conclude that the combination of hydrofoil and elastic plate can effectively generate the thrust force against the wave propagation using wave energy and a variety of thrust force can be generated for a hydrofoil by adjusting the dimension of elastic plate. Because elasticity of the plate directly influences thrust generation of the flapping foil.

Chapter 3 Thrust Force Empirical Formula of a Flapping Foil

3.1 Dimensional analysis

To proceed with the multiple regression analysis of the experimental data, we needed to estimate the non-dimensional numbers. Thus, we opted for a dimensional analysis of the geometrical, environmental, and material properties of the flapping foil experiments. This work was published in [34].

The thrust of the flapping foil depends on the parameters listed in Table 3.1. Where length of elastic plate (L) and breadth of elastic plate (B) are geometric properties of the flapping foil.

Table 3.1 – Parameters that influence the thrust force

Sl. No.	Parameters	Dimension
1	Mass density (ρ)	$M L^{-3}$
2	Breadth of elastic plate (B)	L
3	Length of elastic plate (L)	L
4	Acceleration due to gravity (g)	$L T^{-2}$
5	Wave Height (H)	L
6	Wavelength (L_w)	L
7	Fluid viscosity (μ)	$M L^{-1} T^{-1}$
8	Flexural rigidity of elastic plate (EI)	$M L^3 T^{-2}$
9	Added pitch moment of elastic plate (I_a)	$M L^2$

Mass density (ρ), acceleration due to gravity (g), wave height (H), wave length (L_w), dynamic viscosity of water (μ) and added pitch moment of elastic plate (I_a) represent environmental properties and material properties for the dimensional analysis was represented by the flexural rigidity of elastic plates (EI).

The added pitch moment of elastic plates (I_a) was obtained from the pitch wave radiation of the elastic plates in gravity waves using UOU in-house code. The elastic modulus of the elastic plates (E) was obtained from a small test carried out in the lab. We used an elastic plate of length 14 cm and breadth 8 cm which was clamped at one end like a cantilever beam and applied loads varying from 100 N to 400 N on the free end of the elastic plate and recorded the deflection for all the applied loads. This experiment was repeated two more times and average value was used for the estimation of the elastic modulus of plates ($E = 1.072$ GPa) using the beam theory formula for the cantilever beam. Further, the wave orbital velocity was obtained from the multiplications of incoming wave frequency (ω) and amplitude ($H/2$). Density of water was assumed as 1000 kg/m^3 . The dynamic viscosity of the fresh water (μ) at 25°C was assumed as $8.9 \times 10^{-4} \text{ Pa.s}$. Area of Foil (A_F) and water depth (D) were unchanged through the process of thrust estimation.

Dimensional Analysis:

$$T \propto \rho^a B^b L^c g^d H^e (L_w)^f \mu^g (EI)^h (I_a)^i \quad (1)$$

Total number of variables (m) = 10

Total number of fundamental dimensions (n) = 3

Total number of non-dimensional quantities = $m - n = 7$

$$T = \rho g L^3 f \left\{ \left(\frac{B}{L} \right)^b \left(\frac{L_w}{L} \right)^c \left(\frac{H}{L_w} \right)^e \left(\frac{\mu}{\rho L (gL)^{0.5}} \right)^g \left(\frac{EI}{\rho g L^5} \right)^h \left(\frac{I_a}{\rho L^5} \right)^i \right\} \quad (2)$$

$$\frac{T}{\frac{1}{2} \rho L^2 V^2} = f \left\{ \left(\frac{L}{B} \right)^j \left(\frac{gL}{V^2} \right)^p \left(\frac{H}{L_w} \right)^e \left(\frac{\mu}{\rho V L} \right)^q \left(\frac{EI}{\rho V^2 L^4} \right)^h \left(\frac{I_a}{\rho L^5} \right)^i \right\} \quad (3)$$

Where;

$$V = \frac{\omega H}{2} \quad (4)$$

From dispersion relation,

$$\frac{\omega^2}{g} = \frac{2\pi}{L_w} \tanh\left(\frac{2\pi}{L_w} D\right) \quad (5)$$

Where, Equation 1 shows that the thrust force generated by a flapping foil in waves was directly proportional to the variables shown in the Table 4. Equation 2 shows the arrangement of variables in non-dimensional form using Buckingham-pi theorem. Equation 3 rearranges the dimensionless terms by introducing the velocity into it that shows the total 7 non-dimensional quantities that was reduced from the total 10 numbers of variables. Also, these 7 non-dimensional quantities will be carried for the regression analysis. Equation 4 explains the velocity in which wave frequency (ω) was obtained from the dispersion relation in shallow water for each wave lengths in a given water depth as shown in the Equation 5. In deep water case, the tangent hyperbolic goes very near to 1.

3.2 Multiple regression analysis

The thrust force of a flapping foil depends on the elastic plate and wave conditions. Therefore, the thrust coefficient is considered as a dependent variable, while the aspect ratio, wave slope, Froude number, Reynolds number, elastic plate number, and added mass number are independent variables. The short notations and mathematical presentations of these variables can be found in Table 5. We made sure that all the independent variables were correlated individually with the dependent variable and had a p-value that was smaller than 0.05. Thus, the dependent variable (C_t) can be written as a function of all the independent functions as shown in Equation 6.

$$C_t = f \{Ar, Ws, Rn, Fn, Ep, Ad\} \quad (6)$$

Table 3.2 – Variables for multiple regression analysis

Sl. No.	Variables	Short Notation	Mathematical Expression
1	Thrust coefficient	Ct	$T/0.5\rho(A_F)V^2$
2	Aspect ratio of elastic plate	Ar	L/B
3	Wave slope	Ws	H/L_W
4	Froude number	Fn	V/\sqrt{gL}
5	Reynolds number	Rn	$VL\rho/\mu$
6	Elastic plate number	Ep	$EI/\rho V^2(A_{EP})^2$
7	Added mass number	Ad	$I_a/\rho L^5$

Multiple regression analysis was carried out by using the results of the model tests, as displayed in Figure 2.8. Once the independent variables are finalized and applied to the multiple regression analysis, the multiple regression model yields a value of 92% ($R=0.92$), which is very stable because the difference between them is small. Table 6 shows each coefficient, the standard errors, t-statistics, p-values, and the lower and the upper 95% values. The explanation provided by the multiple regression model is supported because all the p-values are smaller than the significance level of 0.05.

Table 3.3 – Results of regression analysis for the thrust generation of flapping foil

	Coefficients	Standard Error	t Statistic	P-value	Lower 95%	Upper 95%
Intercept	-7.13	1.76	4.06	0.00	3.62	10.64
Fn	191.36	37.87	5.05	0.00	115.66	267.05
Ln (Ep)	-1.57	0.32	-4.88	0.00	-2.21	-0.93
Ad	-1.02	0.27	-3.80	0.00	-1.56	-0.48
Ar	-6.55	2.52	-2.60	0.01	-11.58	-1.52
Ws	-635.99	102.49	-6.21	0.00	-840.86	-431.11
Ws ²	2422.10	606.51	3.99	0.00	1209.70	3634.50
Fn×Ar	-100.19	32.08	-3.12	0.00	-164.31	-36.07
Ln (Ep)×Ar	1.51	0.40	3.74	0.00	0.70	2.31
Ar×Ws	193.16	40.78	4.74	0.00	111.65	274.68

It was found that the Fn and Rn values were strongly correlated. Thus, to avoid multicollinearity, Rn was eliminated from the regression analysis. Because, the foil was flapping owing to orbital velocity of surface waves that was dominated by gravity forces. Thus, Fn was enough to describe the fluid flow. Further, several combinations of independent variables were tested during the analysis and the effective combinations were included in the analysis to improve the correlation of the final form as shown in the Table 6 and Equation 7.

The coefficients for each independent variable can be rounded off so that the final form of the empirical equation can be written as follows;

$$\begin{aligned} \ln(Ct^2) = & -7.13 + 191.36 \times Fn - 1.57 \times \ln(Ep) - 1.02 \times Ad - 6.55 \times Ar - 636 \times Ws + 2422 \times (Ws)^2 \\ & - 100.2 \times Fn \times Ar + 1.51 \times \ln(Ep) \times Ar + 193.16 \times Ar \times Ws \end{aligned} \quad (7)$$

Figure 3.1 shows the comparison of the results between the experiment and the empirical formula. The comparison is shown on a log scale. Even though the distribution of the experimental results does not adhere to an easily defined mathematical form, the results obtained from the empirical formula could elicit a good agreement with the experimental results.

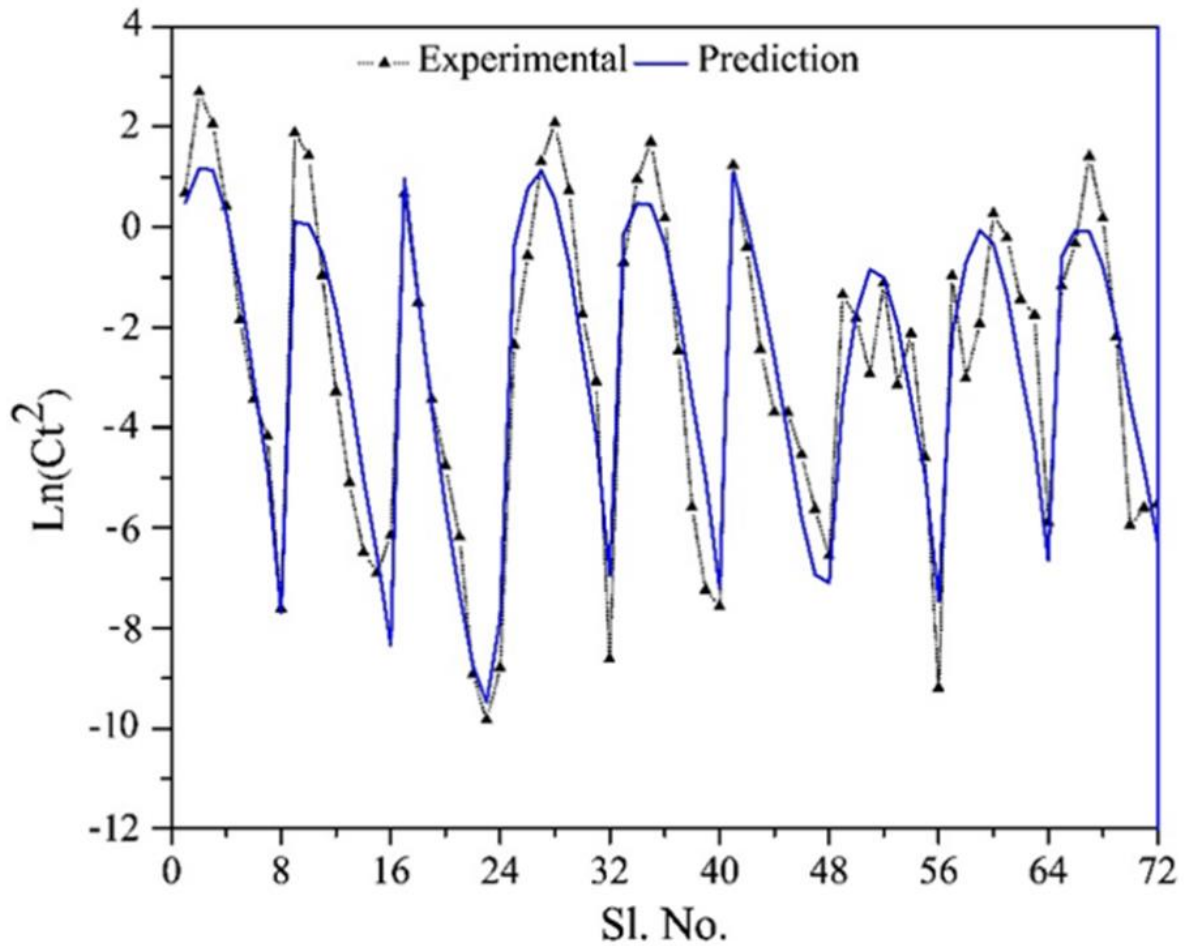


Figure 3.1 – Experimental results compared with the results obtained from the empirical formula

3.3 Verification

We derived an empirical formula as shown in Equation 7, based on our experiments carried out in a wave flume. Where the water depth was restricted to 40 cm. As a solution, we have wave slope as an independent variable for the multiple regression analysis to include the effects of a change in water depth. Further, to validate our method, we carried out a model test with the same model set up in a wide tank (30 m long, 20 m wide, and 2.5 m deep) where the water was comparatively deeper. We used the same hydrofoil attached with an elastic plate of the length 'L2' and breadth 'B2'. Subsequently, we generated four regular incoming waves as shown in the Table 3.4 and measured the thrust force using the same capacity load cell as mounted on the wave flume. The comparison of the results is displayed in Figure 3.2 which shows a good agreement between the experimental and predicted results for the widetank. Therefore, the empirical formula could be useful for the thrust estimation of a passive flapping foil (NACA0015) regardless of any water depths, where the foil was attached to an elastic plate and incoming surface gravity waves excites the flapping motion of the foil using the vertical components of the wave orbital velocity.

Table 3.4 – Load cases for widetank experiments.

Load Case	H(cm)	ω (rad/s)	Wave Number (K)	Wave Slope (Ws)
1	2	4.63	2.18	0.0069
2	3	4.63	2.18	0.0104
3	2	9.24	8.72	0.0277
4	3	9.24	8.72	0.0416

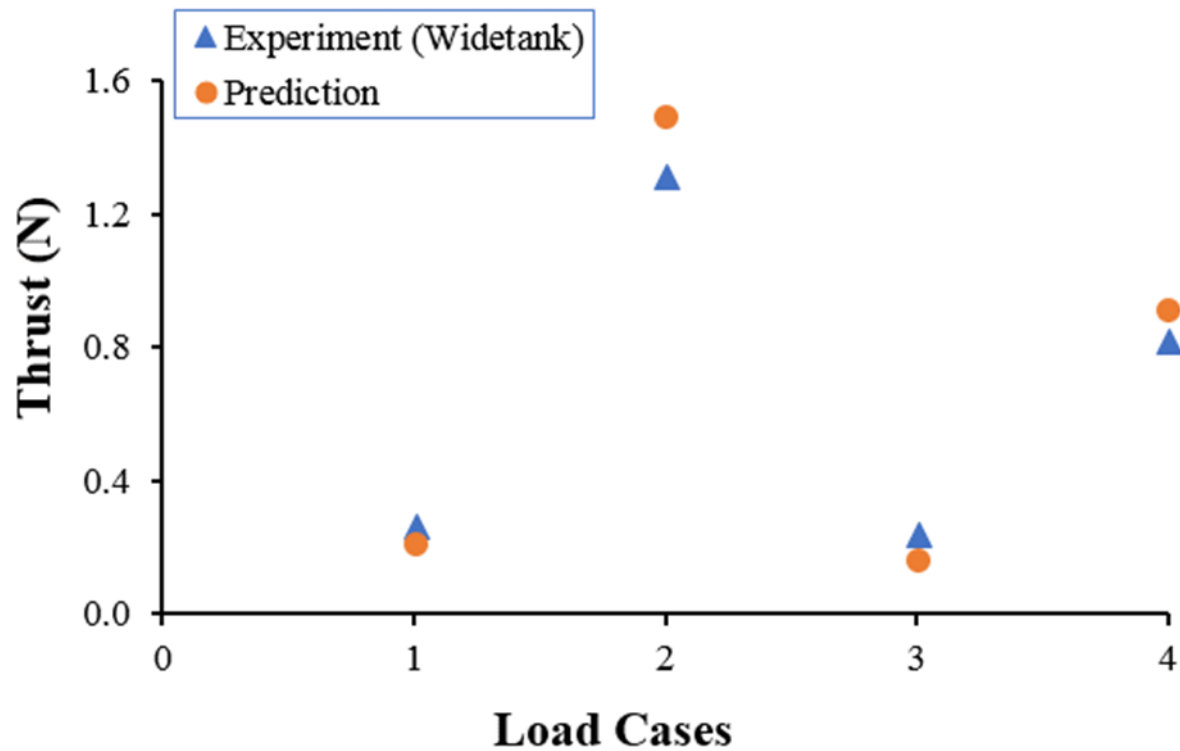


Figure 3.2 – Experimental results in widetank compared with the results obtained from the empirical formula

3.4 Conclusion

In this section, an empirical equation used for the prediction of thrust generated by the flapping foil in regular waves is introduced based on the experimentally recorded data. Therefore, passively flapping thrust forces can be predicted for a given wave conditions using empirical formula that will be useful to design a stationkeeping control system.

Chapter 4 Combination of Foils

This chapter includes the various combinations of flapping hydrofoils and their effects on stationkeeping. Single flapping foil in head waves were studied in detail in previous sections, therefore, a combination it draws attention which is vital for the stationkeeping design. From the previous experiments, the highest thrust (HT) and lowest thrust (LT) producing elastic plates were selected for the combination of foils as displayed in Figure 4.1.

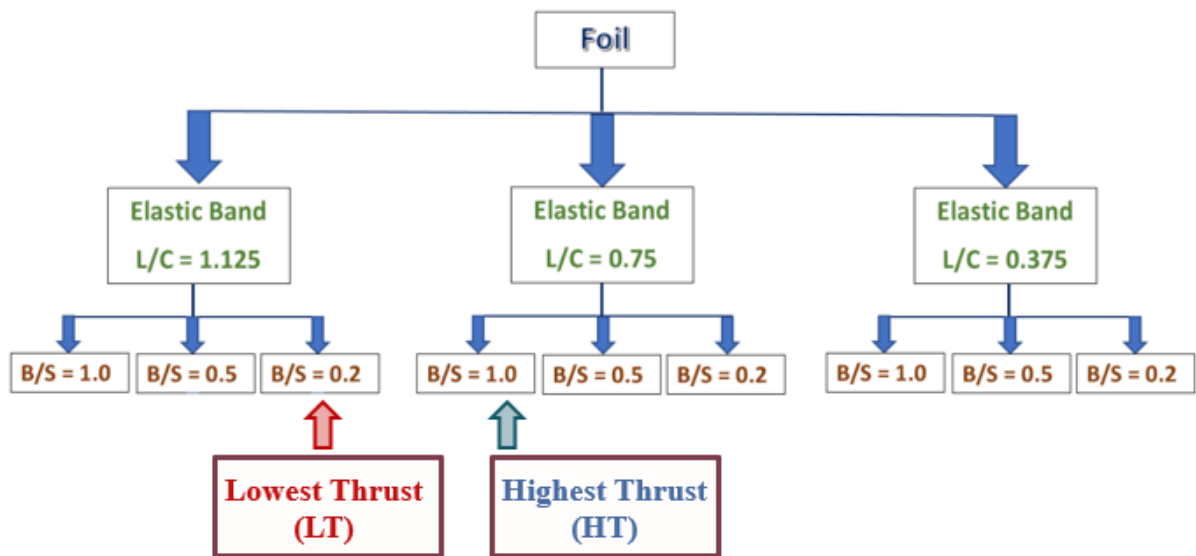


Figure 4.1 – Selection of elastic plates for the combined foil experiments.

4.1 Two flapping foils in waves

This section explains the combination of two flapping foils faced opposite to each other in waves and the experiments were performed in the wave flume, UOU. Since, two foils are acting at the same time, a resultant thrust was measured for a given wave condition.

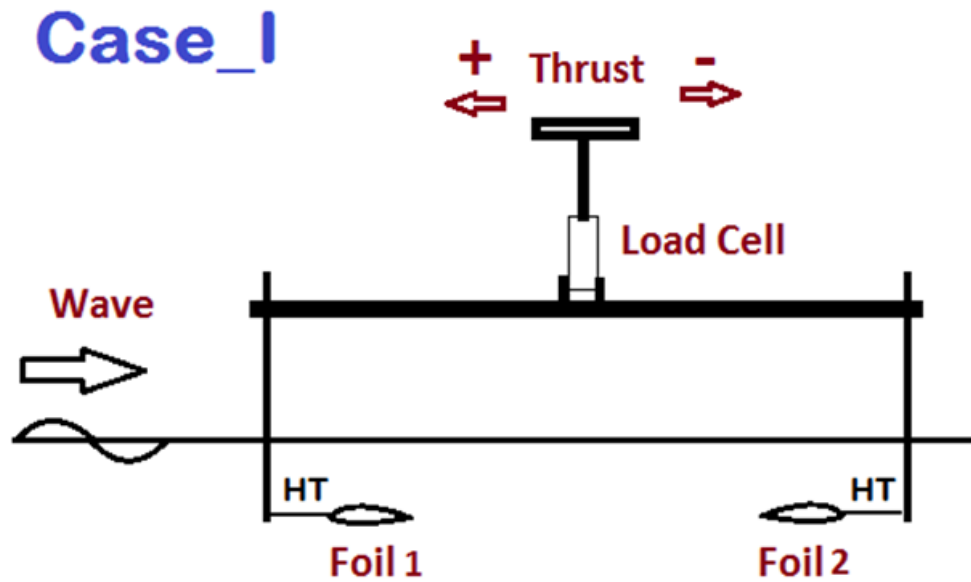


Figure 4.2 – Combination of two highest thrusts (HT).

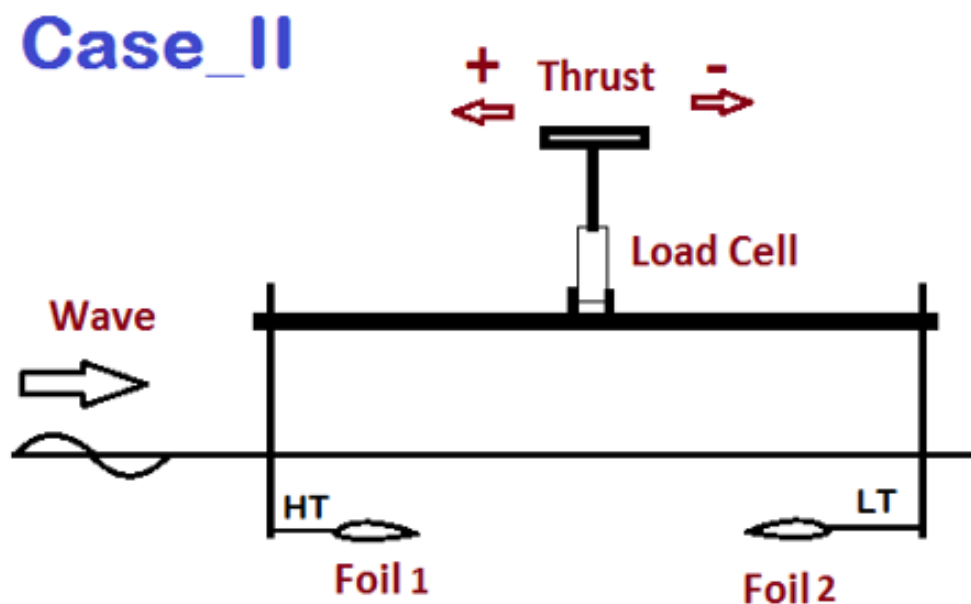


Figure 4.3 – Combination of highest thrust (HT) and lowest thrust (LT).

Figure 4.2 shows the combination of two flapping foils in waves with both highest thrusts elastic plates called case 1. Figure 4.3 shows the combination of one Highest thrust and one

lowest thrust flapping foil called case 2. The resultant thrust forces were measured positive against the wave propagation. The experiments were carried out for the wavelengths varying from 0.26 m to 3.73 m as shown in Table 4.1 and the resultant thrusts were recorded. Figure 4.4 shows the comparison of case 1 and case 2 experimental results. Results confirmed that by changing the elastic plates alone the resultant thrusts can be shifted from negative to positive that can be useful to design a control system of the stationkeeping model.

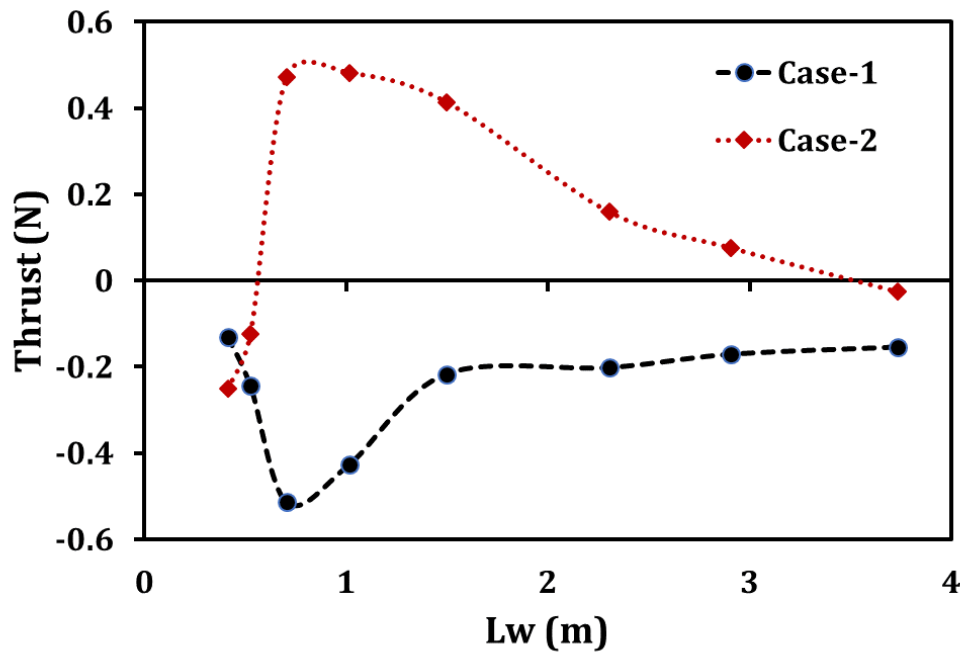


Figure 4.4 – Comparison of case-1 and case-2

4.2 Effects of azimuth angles

From the above experiments, it was confirmed that the resultant thrust forces can be reversed by changing the elastic plates, however, maintaining zero for all the wave conditions was still difficult. More experiments were needed to achieve the zero-drift condition; therefore, effects of azimuth angles were investigated in this sub-section.

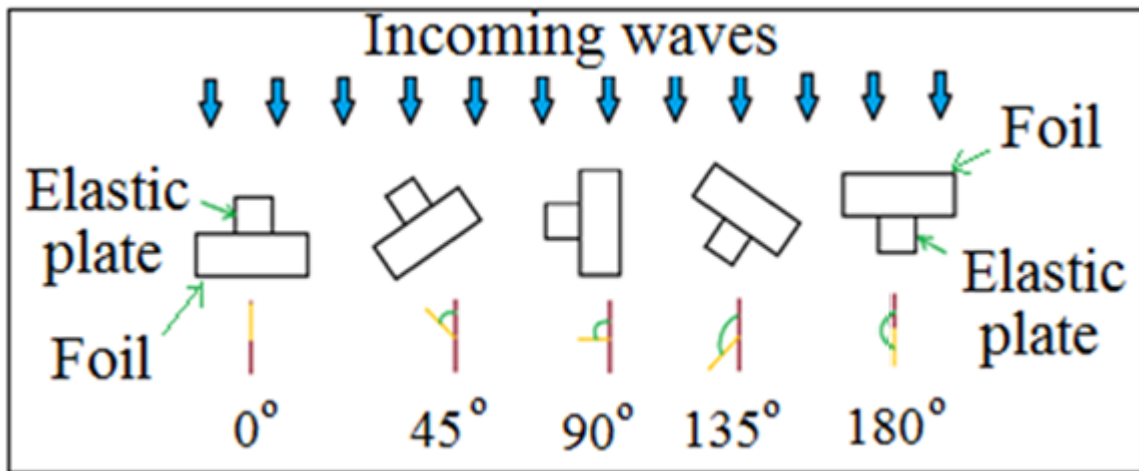


Figure 4.5 - Azimuth angles

Five azimuth angles were investigated as shown in the Figure 4.5 for five load cases as displayed in Table 4.1.

Table 4.1 – Load cases for azimuth angle experiment

RPM	T(s)	Lw(m)	H/Lw	ω (rad/s)
10	2.01	3.69	0.005	3.13
15	1.36	2.30	0.009	4.63
20	1.01	1.49	0.013	6.22
25	0.81	1.01	0.020	7.75
30	0.68	0.72	0.028	9.24

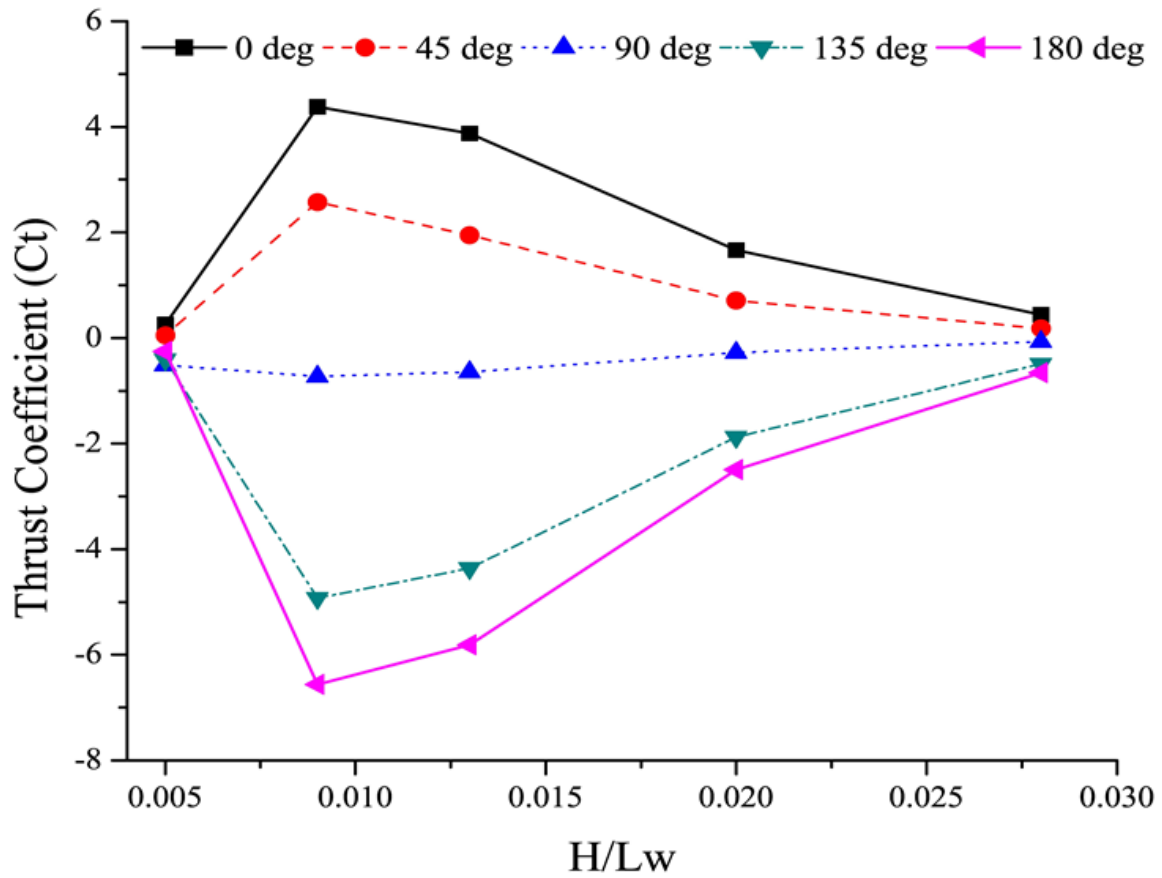


Figure 4.6 – Effects of azimuth angles on thrust

Figure 4.6 shows the effects of azimuth angles on the thrust generation of a passive flapping foil in various wave conditions. Results confirmed that azimuth control can be the fastest method to shift the thrust quantity from positive to negative and vice versa.

4.3 Two flapping plates

To minimize complexity of the experimental model, hydrofoils were replaced by the thin elastic plates as shown in Figure 4.7 and experiments were carried out for the wave conditions displayed in Table 4.2 and the resultant thrusts are shown in the Figure 4.8.

Table 4.2 – Load cases for combined foils experiments.

Case	RPM	Lw (m)	Hw (mm)	Stroke
1	10	3.73	20	140
2	12	3.01	20	152
3	15	2.3	20	155
4	18	1.77	20	172
5	20	1.49	20	175
6	22	1.27	20	178
7	25	1.01	20	180
8	30	0.7	20	185
9	35	0.52	20	187
10	50	0.26	20	188

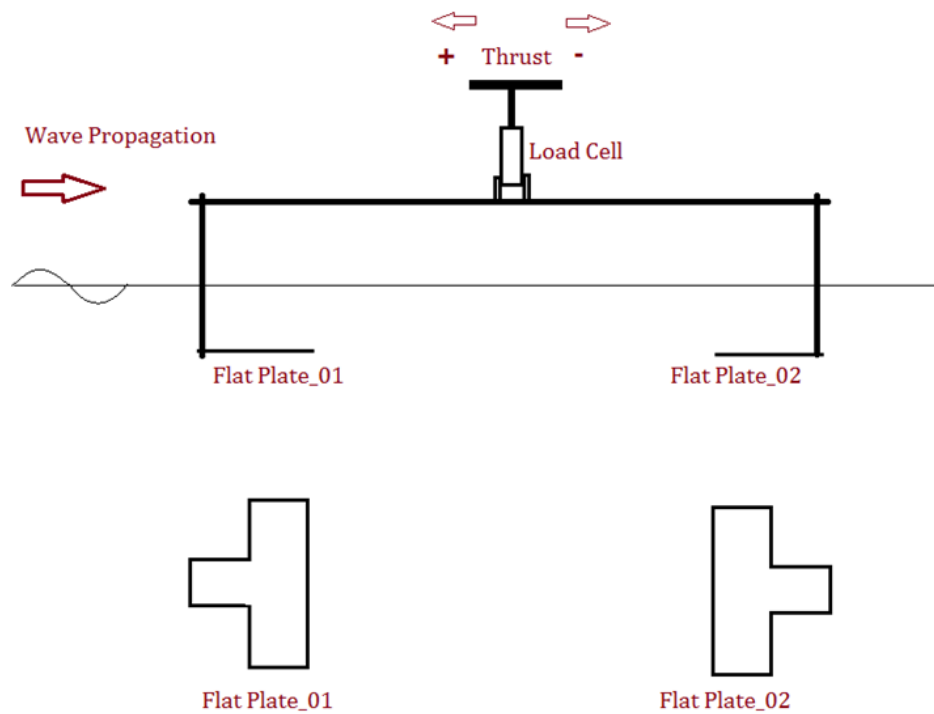


Figure 4.7 – Combination of flapping flat plates

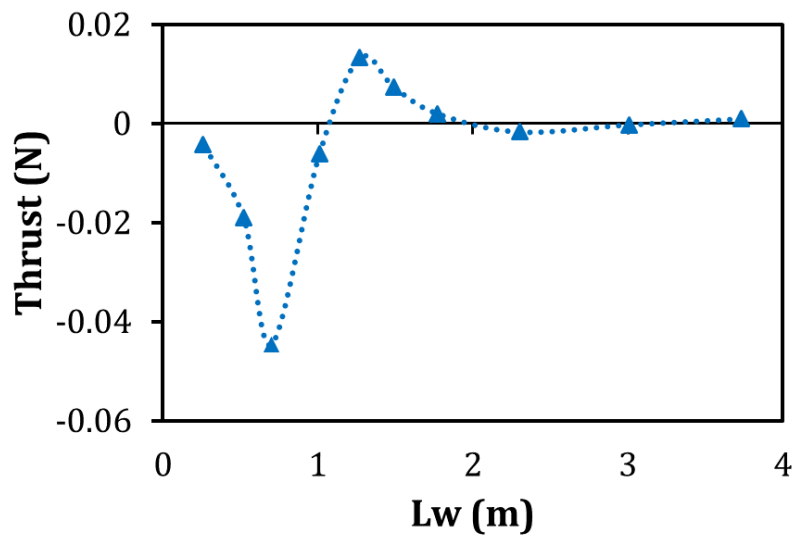


Figure 4.8 – Resultant thrusts due to combination of flapping flat plates

Results show that flapping flat plates keep the zero drift conditions for wavelengths ranging from 1.8 m to 3.7 m but fails to keep the position in shorter waves. Therefore, azimuth control was introduced to keep the position of zero-drift without making changes in the elastic plates and hydrofoils as shown in Figure 4.9 and results are displayed in Figure 4.11.

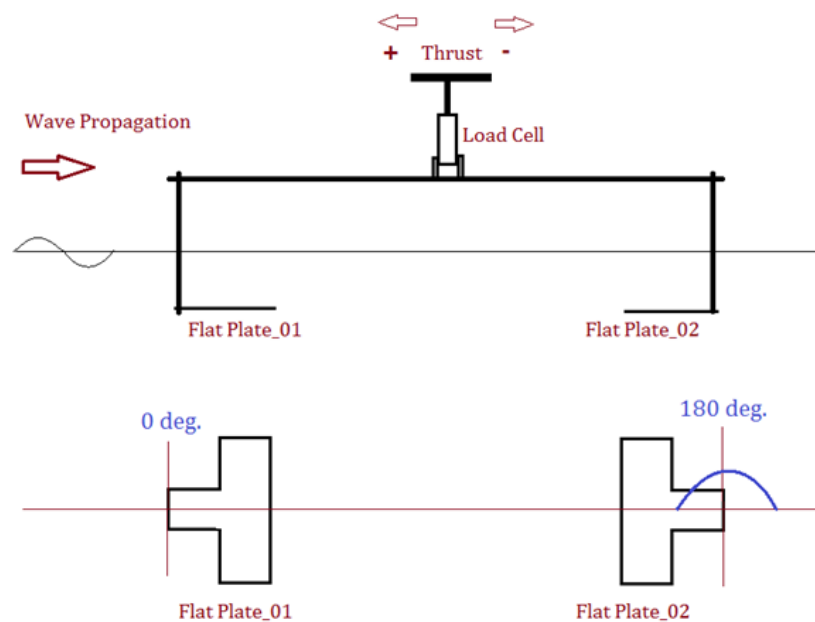


Figure 4.9 – Initial azimuth angles of flapping plates

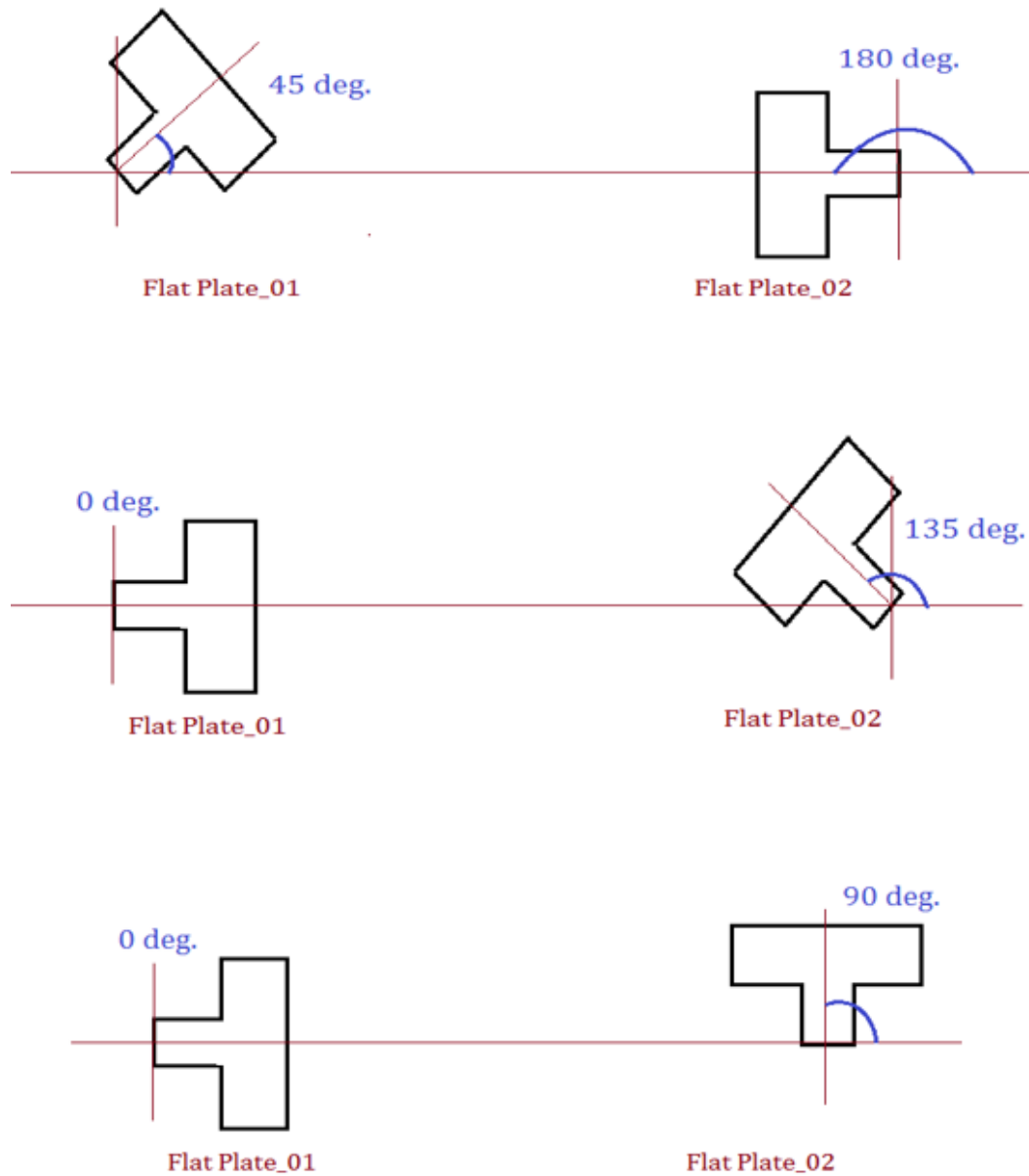


Figure 4.10 – Azimuth angle control

Figure 4.10 shows the azimuth control of the flapping plate stationkeeping system and results prove that azimuth control can be very useful and comparatively easier control option for the flapping foil stationkeeping system.

Table 4.3 – Azimuth control of combined foils experiments.

case	Lw (m)	Plate_01	Plate_02
1	3.73	0	180
2	3.01	0	180
3	2.3	0	180
4	1.77	0	180
5	1.49	45	180
6	1.27	45	180
7	1.01	0	135
8	0.7	0	45
9	0.52	0	90
10	0.26	0	135

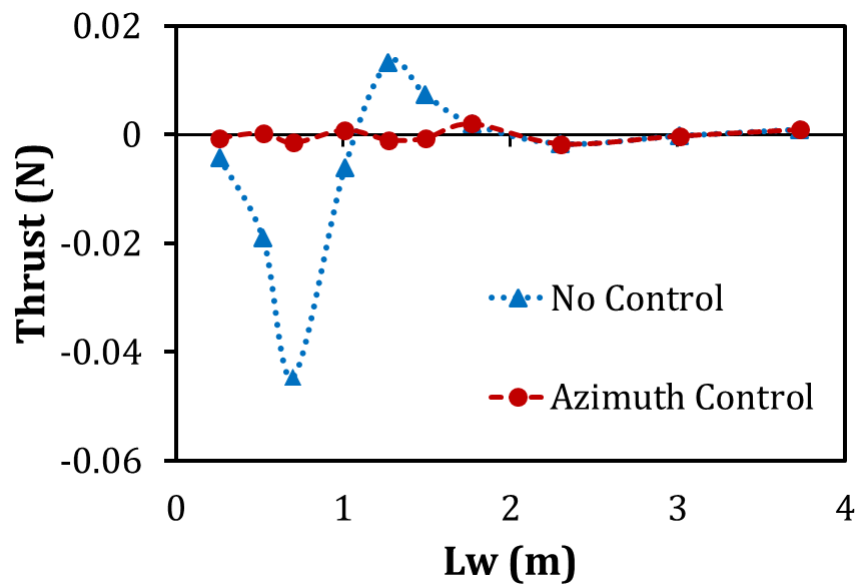


Figure 4.11 – Effects of azimuth control on stationkeeping

4.4 Multiple foils arranged in a circle

This section includes the effects of multiple flapping foils arranged in a circle as shown in the Figure 4.12. This experiment was carried out in widetank, UOU.

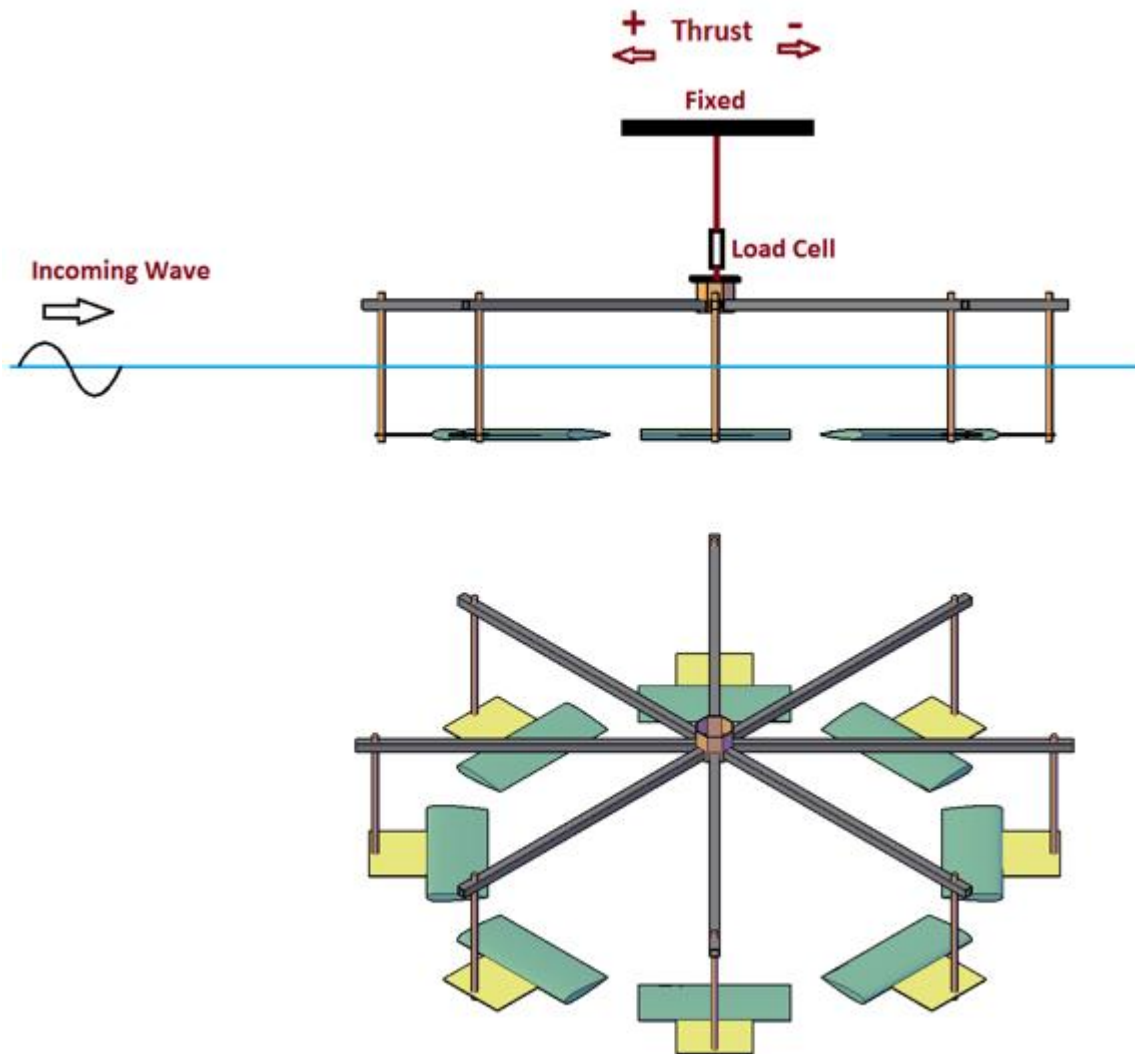


Figure 4.12 – Multiple flapping foils arranged in a circle

Table 4.4 – Load cases for the experiments in widetank, UOU.

Load Case	λ (m)	ω (rad/s)	A (mm)
1	0.95	8.03	35.26
2	1.25	7.03	29.58
3	1.58	6.25	36.14
4	2.36	5.11	30.96
5	3.82	4.01	32.48
6	5.00	3.51	29.64
7	5.64	3.31	24.61
8	6.32	3.12	25.48
9	7.02	2.96	29.68
10	7.90	2.79	20.53

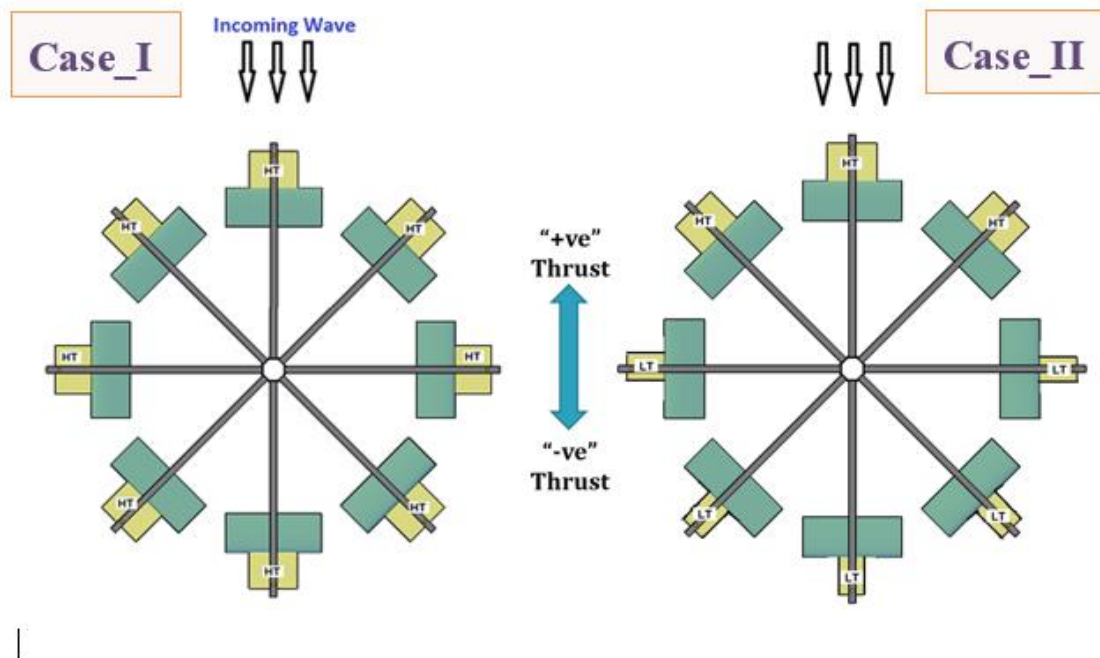


Figure 4.13 – Two cases of stationkeeping model

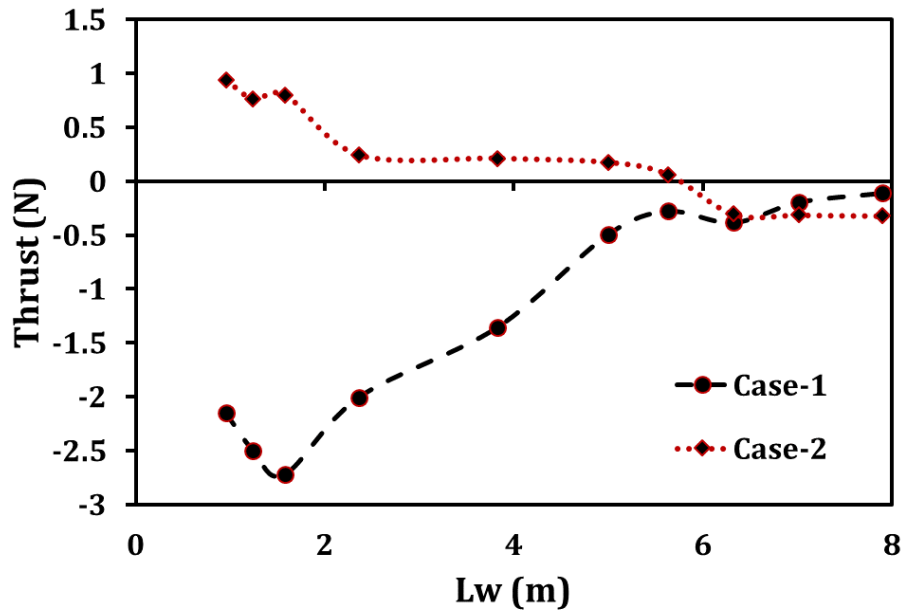


Figure 4.14 – Results comparison of case-1 and case-2

Figure 4.13 shows the combination of eight highest thrust (HT) foils as case-1 and combination of three forward highest thrust (HT) foils and remaining five lowest thrust (LW) foils as case-2. Figure 4.14 shows the comparison of the resultant thrusts of case-1 and case-2. Results shows that the combination of highest thrust (HT) and lowest thrust (LT) performs better in waves.

4.5 Fish cage with multiple foils and plates

The experiments were begun with an idea of implementing renewable methods for the stationkeeping of a very large floating structure. And, we carried out several experiments with 16 flapping foils (NACA0015) attached around a floater as shown in Figure 4.15. The diameter and draft of the floater were 160 cm and 46 cm respectively. The span (S) and Chord (C) were 20 cm and 8 cm respectively. The experiments were carried out in the widetank of the University of Ulsan. The widetank was 30 m long, 20 m wide, and 2.5 m deep. A wave-maker was located at one end of the tank to generate the desired waves. At the other end of the tank, a wave absorbing beach was used as shown in Figure 4.16. Later, we replaced the hydrofoils with 0.5 cm thick flat plates and repeated the experiments.

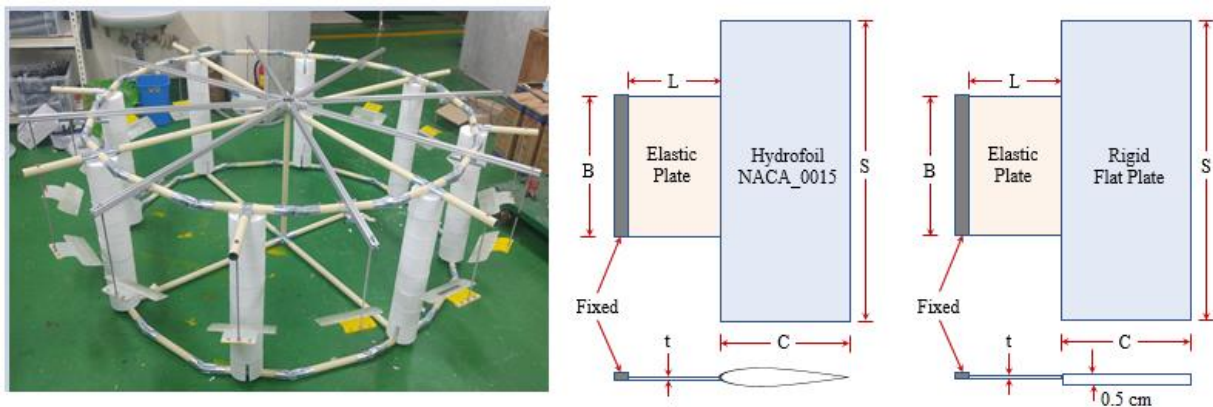


Figure 4.15 – Experimental results in widetank compared with the results obtained from the empirical formula

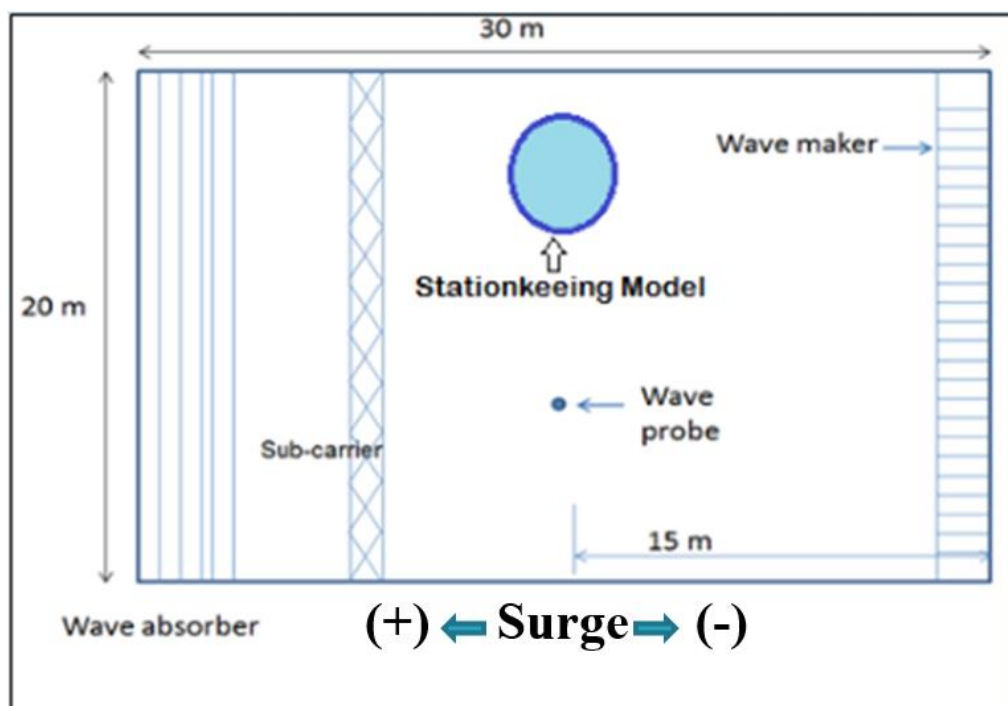


Figure 4.16 – Experimental results in widetank compared with the results obtained from the empirical formula

Table 4.5 – Azimuth control of combined foils experiments.

Case	T(sec)	Wavelength (m)	Wave height (mm)
1	0.8	1.0	34
2	0.9	1.3	31
3	1.0	1.6	28
4	1.2	2.4	31
5	1.6	3.8	32
6	1.8	5.0	24
7	2.0	6.3	30
8	2.1	6.8	24
9	2.3	7.9	29
10	2.5	9.2	27

Figure 4.17 shows the drift in surge direction of the floater attached with 16 flapping foils in waves. Drift along the wave direction was recorded as positive surge as shown in Figure 4.16. Figure 4.18 shows the effects of flapping plates on the drift of the floater in surge direction.

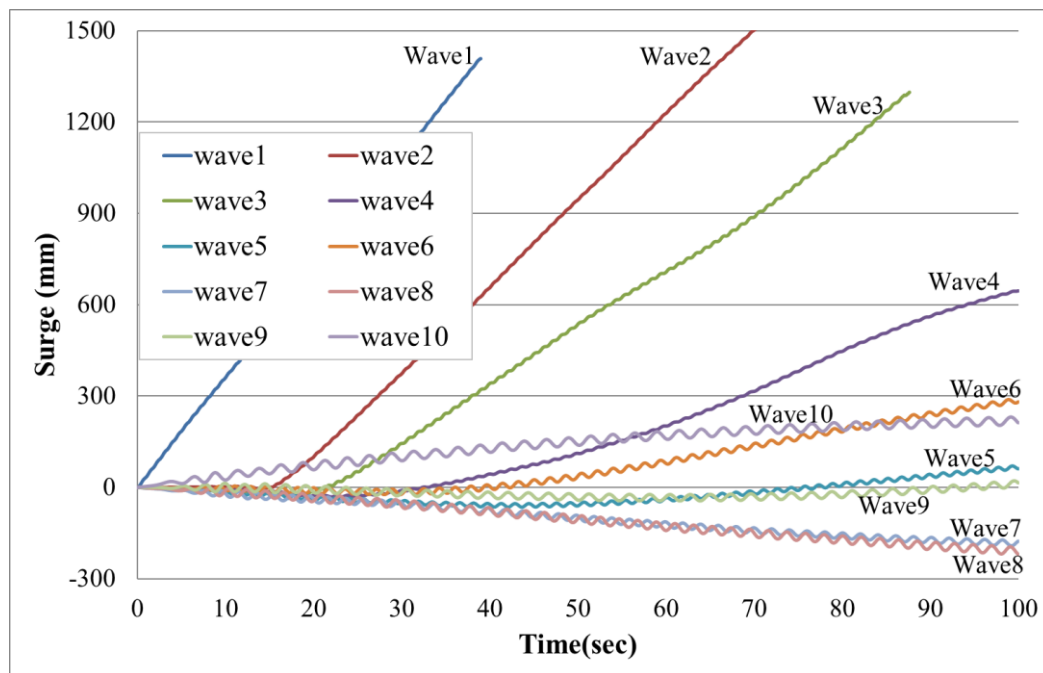


Figure 4.17 – Experimental results in widetank compared with the results obtained from the empirical formula

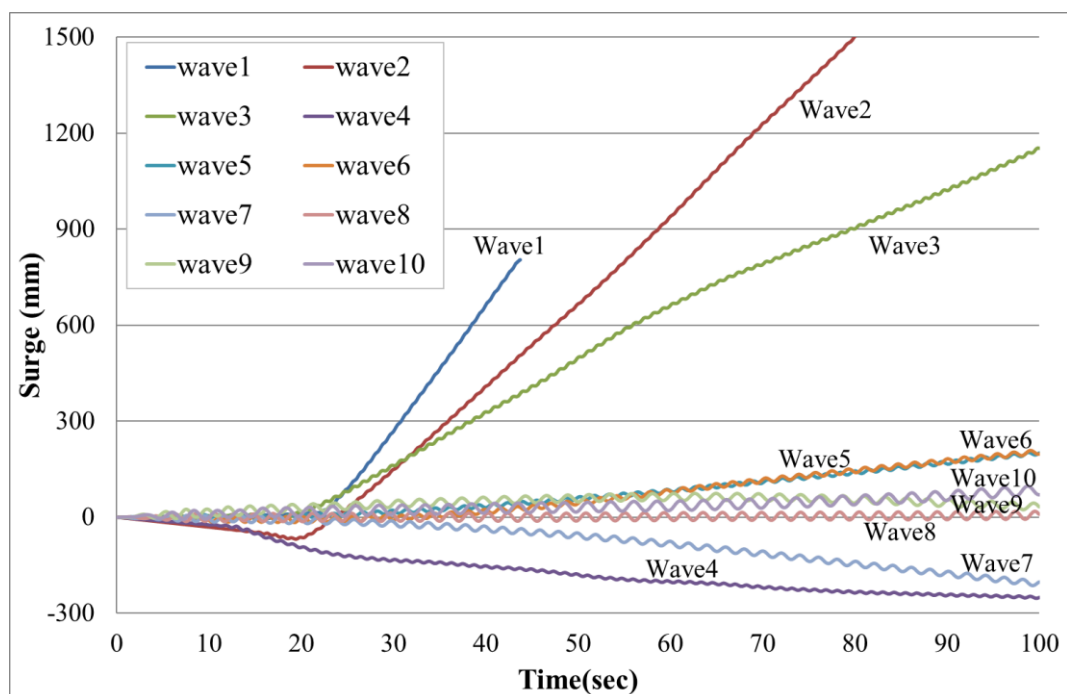


Figure 4.18 – Experimental results in widetank compared with the results obtained from the empirical formula

4.6 Conclusion

We observed that the stationkeeping performance of the floater was better with flapping plates compared to flapping foils. Because, the drifts of the floater with flapping plates were closer to zero for most of the wave conditions except short waves. Therefore, an advantage of flapping plates over flapping foils for the stationkeeping of a floater can be confirmed. And, a detail investigation of the thrust force generated by the flapping plate in waves is required. Also, azimuth control was better in terms of maintaining the position compared to elastic plates, therefore, a detailed investigation of azimuth angle control was needed.

Chapter 5 Passive Flapping Plate in Waves

In this study, the hydrofoil is replaced by the flat plates to minimize the complexity of the structure, that is undergoing harmonic flapping motion. Also, one end of the flat plate was fixed to the tank so that the plate could flap only owing to the incoming waves at a set location. Thrust force generated due to the flapping motion of flat plates in a wave flume was measured experimentally, and the effects of the elasticity and the size of the plates have been discussed in detail. Furthermore, an empirical formula was introduced to predict the thrust force of the flapping plates based on the experimental results using multiple regression analysis.

5.1 Experiment setup

The flapping plate experiments were carried out in a wave flume in the Ocean Engineering Lab, University of Ulsan. The flume was 35 m long, 0.5 m wide, and 0.6 m deep.

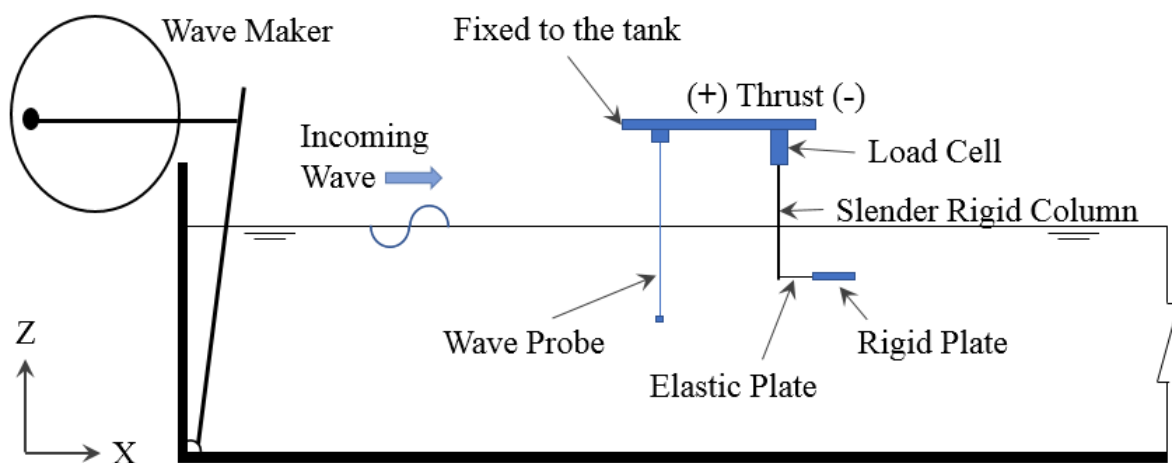


Figure 5.1 – Experimental setup in wave flume

A wave-maker was located at one end of the tank to generate the desired waves. At the other end of the tank, a wave absorbing beach was used to dissipate the wave energy and reduce wave reflection. The water depth and submergence of the plate were, respectively, equal to 0.4 m and 0.05 m and were unchanged during the experiments.

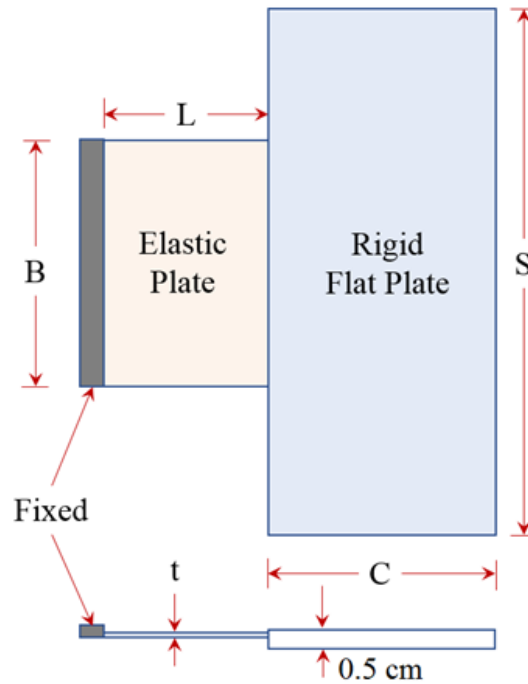


Figure 5.2 – Flapping flat plate

A wave probe was mounted on the fixed frame of a tank, which was positioned 3 m away from the wave paddle. The wave probe was able to measure the water level fluctuations to the nearest 0.5 mm. The diameter of the probe wire was 0.3 cm and its placement in the water before the flapping foil did not cause any significant modification to the wave field. A load cell was mounted on the fixed frame of the tank, which was positioned 0.2 m from the wave probe. The load cell was able to measure the thrust forces in the x-direction of the wave flume as shown in Figure 5.1. The maximum capacity of the load cell was 10 N and was changed to 0.2 N to increase the accuracy of the measurements. The load cell was set to produce 100 observations per second. In general, the load cell was used to record the thrust force of the flapping plate, whereby the flapping plate was attached to the load cell through a slender rigid column. Therefore, a thrust force generated by a flapping plate was experienced by the slender rigid

column, which transferred the thrust force to the load cell to record it. Thrust forces measured along the direction opposite to the incident wave were recorded as positive, and the forces measured along the direction of the wave, as negative.

5.2 Thrust force measurements

The thrust measured in the same manner it was measured for flapping hydrofoil, discussed in chapter-2 of this thesis. Table 5.1 shows the load cases employed on the flapping flat plate. The wavelength varies from 0.41 m to 3.69 m and total 7 cases are recorded for each model. The wave height was kept constant as 20 mm during the experiments.

Table 5.1 – Load cases

Serial Number	RPM	Period (s)	Status	K	ω (rad/s)	Lw (m)
1	10	2.0	Finite	1.7	3.13	3.69
2	15	1.4	Finite	2.7	4.63	2.30
3	20	1.0	Finite	4.2	6.22	1.49
4	25	0.8	Finite	6.2	7.75	1.01
5	30	0.7	Deep	8.7	9.24	0.72
6	35	0.6	Deep	12.0	10.86	0.52
7	40	0.5	Deep	15.5	12.32	0.41

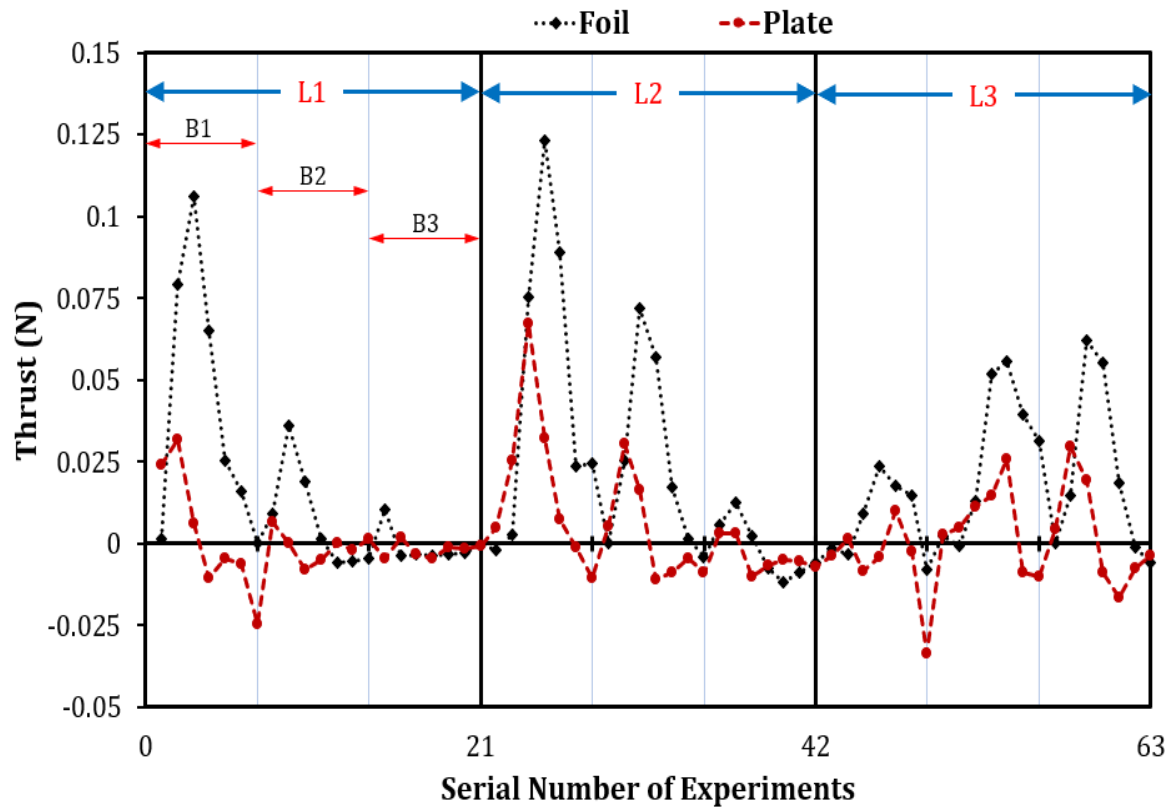


Figure 5.3 – Experimental results and comparison

Figure 5.3 presents the experimental results of the flapping plate for 20 mm heights of waves. The Y-component represents the thrust forces in Newton and the X-component represents the first seven load cases of Table 5.1 are repeated for 9 experiment models shown in the experiment plan Figure 2.6. Therefore, it is represented as “serial number of experiments”. Additionally, a comparison of the thrust generation of a flapping foil and flapping plate is displayed.

5.3 Empirical formula for thrust force

Dimensional analysis was performed to minimize the number of variables.

Table 5.2 – Parameters that influence thrust force.

Sl. No.	Parameters	Dimension
1	Mass density (ρ)	$M L^{-3}$
2	Breadth of elastic plate (B)	L
3	Length of elastic plate (L)	L
4	Acceleration due to gravity (g)	$L T^{-2}$
5	Wave Height (H)	L
6	Wavelength (L_w)	L
7	Fluid viscosity (μ)	$M L^{-1} T^{-1}$
8	Flexural rigidity of elastic plate (EI)	$M L^3 T^{-2}$
9	Added pitch moment of elastic plate (I_a)	$M L^2$

Dimensional Analysis:

$$T \propto \rho^a B^b L^c g^d H^e (L_w)^f \mu^g (EI)^h (I_a)^i \quad (1)$$

Total number of variables (m) = 10

Total number of fundamental dimensions (n) = 3

Total number of non-dimensional quantities = m - n = 7

$$T = \rho g L^3 f \left\{ \left(\frac{B}{L} \right)^b \left(\frac{L_w}{L} \right)^c \left(\frac{H}{L_w} \right)^e \left(\frac{\mu}{\rho L (gL)^{0.5}} \right)^g \left(\frac{EI}{\rho g L^5} \right)^h \left(\frac{I_a}{\rho L^5} \right)^i \right\} \quad (2)$$

$$\frac{T}{\frac{1}{2}\rho L^2 V^2} = f \left\{ \left(\frac{L}{B} \right)^j \left(\frac{gL}{V^2} \right)^p \left(\frac{H}{L_w} \right)^e \left(\frac{\mu}{\rho V L} \right)^q \left(\frac{EI}{\rho V^2 L^4} \right)^h \left(\frac{I_a}{\rho L^5} \right)^i \right\} \quad (3)$$

Where;

$$V = \frac{\omega H}{2} \quad (4)$$

From dispersion relation,

$$\frac{\omega^2}{g} = \frac{2\pi}{L_w} \tanh \left(\frac{2\pi}{L_w} D \right) \quad (5)$$

Where, Equation 1 shows that the thrust force generated by a flapping foil in waves was directly proportional to the variables displayed in Table 5.2. Equation 3 rearranges the dimensionless terms by multiplying the acceleration due to gravity (g) in the numerator and denominator of the 2nd functional term in the right-hand side of the equation and introducing the square of the wave orbital velocity (V^2) in place of “ gL_w ” that shares the same dimension.

Multiple regression analysis was carried out by using the results of the model tests, as displayed in Fig. 5.3. Once the independent variables are finalized and applied to the multiple regression analysis, the multiple regression model yields a value of 85% ($R = 0.85$), which is very stable because the difference between them is small. Right side of equation 3 shows each coefficient, the standard errors, t-statistics, and p-values. The explanation provided by the multiple regression model is supported because all the p-values are smaller than the significance level of 0.05.

It was found that the F_n and R_n values were strongly correlated. Thus, to avoid multicollinearity, R_n was eliminated from the regression analysis. Because, the plate was flapping owing to orbital velocity of surface waves that was dominated by gravity forces. Thus, F_n was enough to describe the fluid flow.

Table 5.3 – Results of regression analysis

	Coefficients	Standard Error	t Stat	P-value
Intercept	29.1	3.877	2.273	0.0003
Fn	461.5	25.605	-4.402	0.0000
Ln(Ep)	-1.8	1.301	0.922	0.0000
Ad	-1e-8	0.512	-0.530	0.0001
Ar	-18.9	5.215	-3.704	0.0005
Ws	-1437	23.65	-2.36	0.0000
(Ws) ²	26554	0.138	-2.533	0.0007
Fn×Ar	198.6	63.560	0.820	0.0002
Ln(Ep)×Ar	1.7	0.840	3.442	0.0011
Ar×Ws	94.6	95.804	0.321	0.0007

The coefficients for each independent variable can be rounded off so that the final form of the empirical equation can be written as follows;

$$\ln(Ct^2) = 29.1 - 461.5 \times Fn - 1.8 \times \ln(Ep) - 1e-8 \times Ad - 18.9 \times Ar - 1437 \times Ws + 26554 \times (Ws)^2 + 198.6 \times Fn \times Ar + 1.7 \times \ln(Ep) \times Ar + 94.6 \times Ar \times Ws \quad (6)$$

Figure 5.4 shows the comparison of the results between the experiment and the empirical formula. The comparison is shown on a log scale. Even though the distribution of the experimental results does not adhere to an easily defined mathematical form, the results

obtained from the empirical formula could elicit a good agreement with the experimental results.

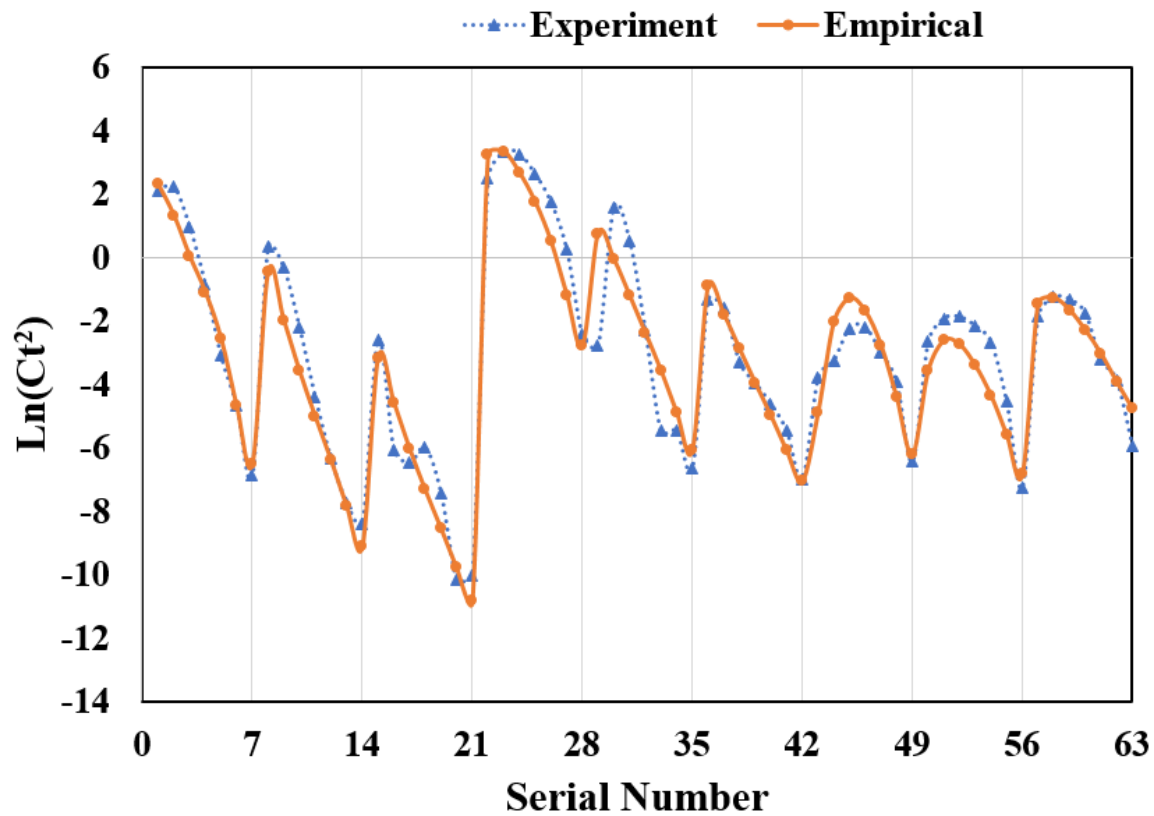


Figure 5.4 – Experimental results compared with the results obtained from the empirical formula

5.4 Conclusion

In this study, thrust force generated by the flapping motion of a rigid plate attached to an elastic plate in the presence of waves was investigated experimentally, whereby the plate could flap at a fixed location using wave energy. Based on the measurement of thrusts experimentally, an

empirical equation used for the prediction of thrust generated by the flapping plate in regular waves is introduced. Finally, the following conclusions were drawn based on this study.

1. Flapping foil generates greater thrust compared to flapping plate in waves, that is ideal for the propulsion. However, the thrust generation of the flapping foil was very unstable in the range of wave lengths. Also, the hydrofoil was a comparatively complex geometry. Therefore, flapping plates have advantages over the flapping foils for the design of a passive stationkeeping system in waves.
2. The thrust forces of the flapping plate attached to an elastic plate can be predicted using the empirical formula.

Chapter 6 FSI Numerical Simulation Using CFD

This chapter aims at analyzing the fluid-structure interaction of a horizontally placed passive flapping foil in regular waves. A rigid NACA 0015 section of 8 cm chord length, made of acrylic glass was attached from its leading edge to the 0.1 cm thick high-density polyethylene (HDPE) elastic plate as shown in Figure 6.1.

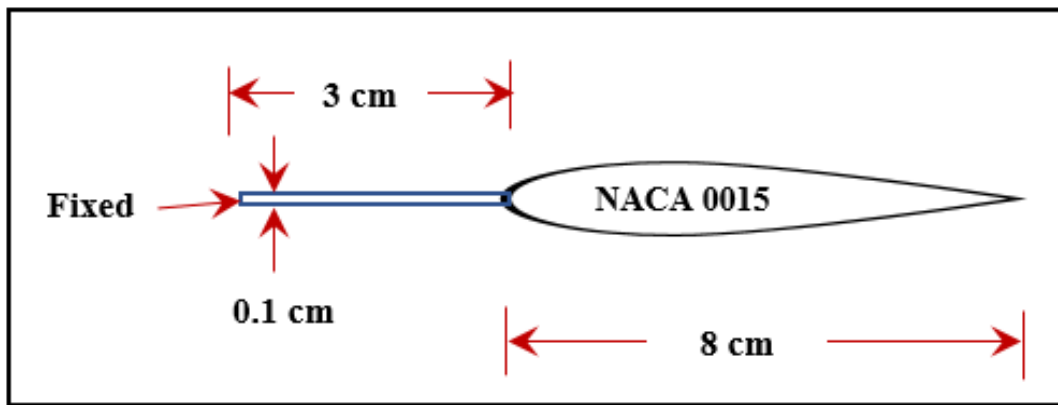


Figure 6.1 – Flapping foil

6.1 Modelling

2-way FSI simulations for the passive mode of flapping foil were done using ANSYS Workbench 19.2 [35]. Since the current version of ANSYS doesn't support the FSI simulation for 2-Dimensional models, 1 cm thick geometry consists of fluid and solid domain was created for the simulation. Duration of the simulation was 7 seconds.

Geometrical models of both flapping foil and fluid domain are created as shown in Figure 6.2. The fluid domain consists of two mediums (air and water). Length of the rectangle was six times of the wavelength (λ) and the structural model was placed at 2λ distance from the inlet

and 5 cm below the mean free surface line. Water depth was considered as 40 cm as shown in Figure 6.2. Elastic plate (0.1 cm thick) was fixed at one end and from another end, it was attached to the leading edge of the hydrofoil. The material properties of the hydrofoil and elastic plate were as acrylic glass and HDPE respectively.

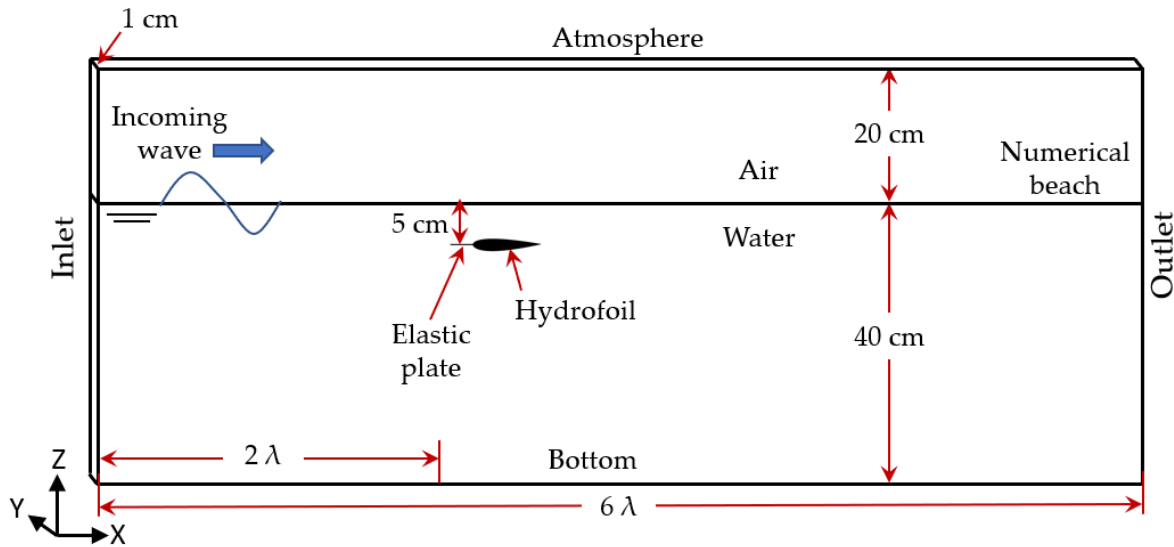


Figure 6.2 – Geometry of fluid domain

6.2 Computational mesh

The volume of the fluid domain was formed using FLUENT Mesh. It was made up of tetrahedral cells belonging to the unstructured mesh category. A box of the very fine mesh was created from inlet to capture the free surface and the structural deformation effectively. Also, the volume mesh of the fluid domain includes the inflation layer around the flapping foil to resolve the boundary layer effects efficiently in turbulent flow as shown in Figure 6.3. The growth ratio of inflation layer was used as 1.2 to maintain a slow transition of meshes. The fluid mesh contains 2.5 million cells.

6.2.1 Near wall treatment

In order to get a good solution for a wall under dynamic loading, the distance from the wall to the first cell is considered an important parameter, obtained from a non-dimensional number

y^+ . The target value of y^+ was evaluated from the ANSYS Fluent simulation as 1. Therefore, the first layer thickness of inflation evaluated as 0.85 mm.

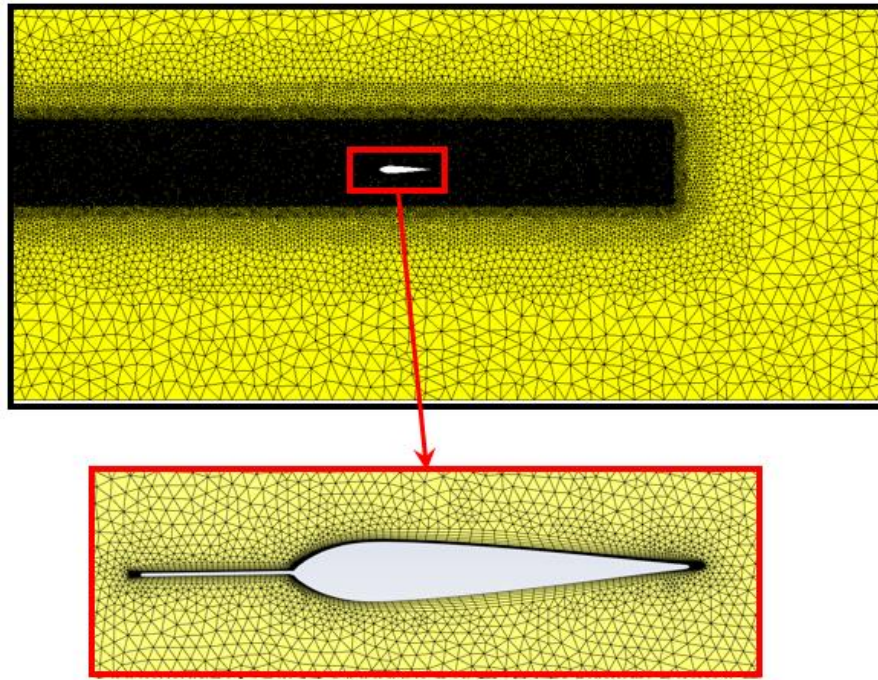


Figure 6.3 – Mesh of fluid domain

6.2.2 Structured mesh

The volume of the solid domain was formed using Structural Mesh. It was made up of hexahedral cells belonging to the structured mesh category as shown in Figure 6.4. The solid mesh contains 25 thousand cells.

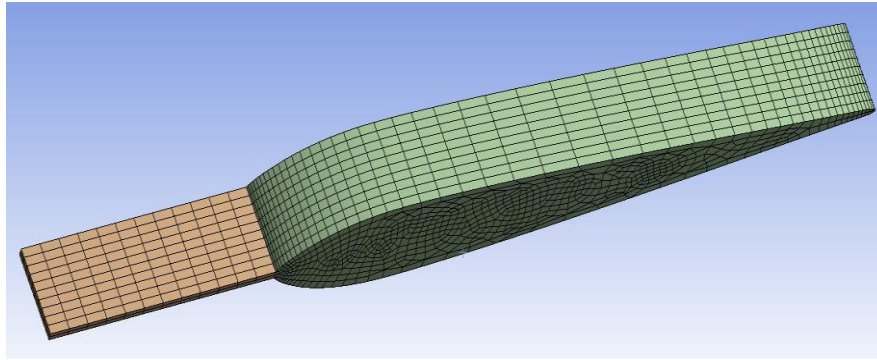


Figure 6.4 – Mesh of solid domain

6.2.3 Load cases

There are four wave conditions are simulated using CFD tool as shown in the Table 6.1.

Table 6.1 – Load cases for CFD simulation

Load case	λ (m)	T (s)	ω (rad/s)
1	0.52	0.58	10.86
2	1.01	0.81	7.75
3	1.49	1.01	6.22
4	2.30	1.36	4.63

6.2.4 Modal acoustic analysis

Modal acoustic analysis was performed to determine the natural flapping frequency of the foil in air and water [36] as shown in Figure 6.5. It is an essential process to avoid any structural failure due to the resonance.

In order to evaluate the natural frequencies of a flapping foil in air and water, an acoustic body of fluid around the flapping foil was created. The used model is shown in Figure 6.5. Figure 6.6 shows the 380,000 tetrahedral mesh generated for the acoustic body and Figure 6.7 shows

the 10,000 hexahedral mesh generated for the solid structure. The interface of solid and acoustic body element nodes was shared to avoid contact elements. The modal acoustic analysis was performed in full damping mode. The natural period of the flapping foil was estimated as 0.15 sec in air and 0.23 sec in water.

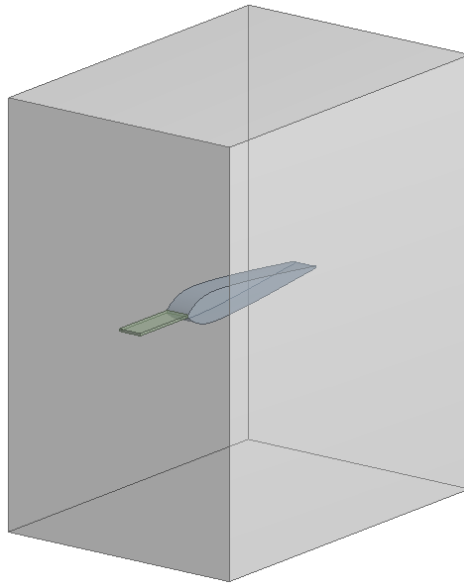


Figure 6.5 – Model of acoustic body

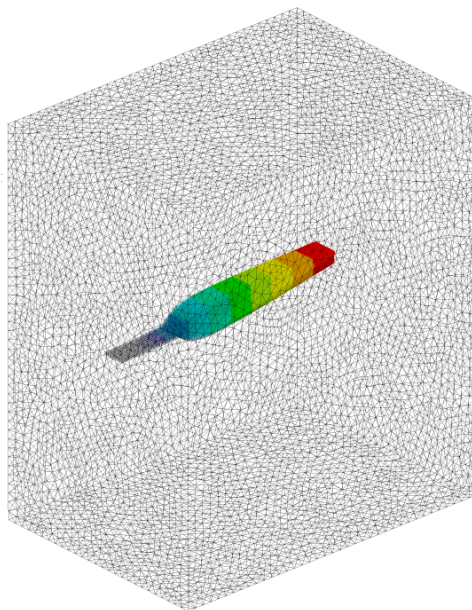


Figure 6.6 – Mesh of acoustic body

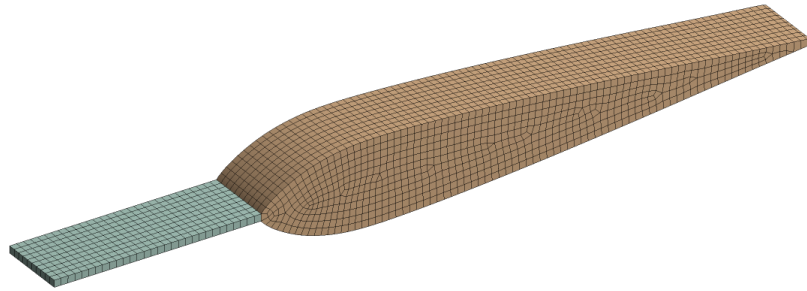


Figure 6.7 – Mesh of flapping body

6.3 Solver settings

The 2-way FSI simulation was conducted to evaluate the thrust forces due to active flapping motion of the hydrofoil in regular waves.

6.3.1 Boundary conditions

Table 6.2 shows the conditions applied to the boundaries of the fluid domain.

Table 6.2 – Boundary conditions of fluid domain

Domain	Boundary condition
Inlet	Velocity-inlet (open channel wave boundary)
Outlet	Pressure-outlet (Numerical beach)
Atmosphere	Wall (zero shear)
Flapping Foil	Wall (no slip)
Side wall	Symmetry
Bottom	Wall (zero shear)

6.3.2 Fluent solver setup

Fluent uses the finite volume method to convert the general transport equation into a system of algebraic equations. The Reynolds Averaged Navier Stokes (RANS) was used to model the effects of turbulence. K- ω SST (Shear Stress Transport) turbulence model was used to effectively capture the near the wall flow and free surface flow regions as shown in Table 6.3.

Table 6.3 – solver setup

Air density	1.225 kg/m ³
Water density	998.2 kg/m ³
Turbulence model	k- ω SST
Multiphase model	Volume of fluid
Scheme	implicit
Wave theory	2 nd order stokes
Pressure velocity coupling	SIMPLE
Flow	Open channel flow
Momentum	2 nd order upwind
Volume fraction	compressive
Pressure	PRESTO
Turbulent kinetic energy (k)	2 nd order upwind

6.3.3 System coupling setup

System coupling tool was used to integrate fluid and structural solvers in FSI simulations. Figure 6.8 shows how ANSYS fluid solver (FLUENT) and ANSYS solid solver (MECHANICAL) are coupled and the information transferred.

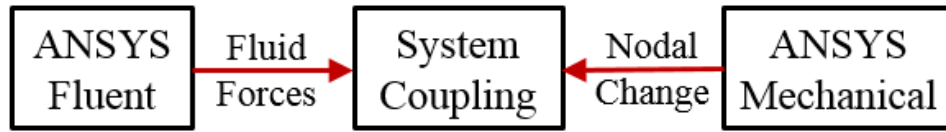


Figure 6.8 – System coupling flow chart

Fluent provides information on the fluid forces acting on the body and Mechanical provides nodal displacement changes in the structure due to fluid loading and system coupling synchronize the whole setup of simulation. This type of simulation called 2-way FSI. The step size for the simulation was used as 0.0005 seconds.

6.4 Results

Thrust forces obtained for the passive mode of the flapping foil in a numerically modelled 1 cm thick fluid-solid domain as shown in Figure 6.2 and the end effects of the flapping foil was neglected. The span of the flapping foil was 20 cm during the experiment, therefore all the numerically obtained results were multiplied 20 times and presented in this paper. The global forces acting on the flapping foil in x-direction of the wave flume was considered as thrust force. However, in the results section, the thrust forces are varying in the y-direction of the plots. The positive y-direction of the thrust plot represents the force generated against the wave direction.

6.4.1 Mesh convergence

In order to perform a mesh convergence study, three mesh resolutions were created as mentioned in Table 6.4. Mesh convergence check was performed in ANSYS FLUENT 19.2 by generating a regular wave. And the forces acting on the fixed foil in x and z directions were evaluated as shown in Figure 6.9 and Figure 6.10 respectively.

Table 6.4 – Mesh resolution

Mesh resolution	Number of elements
Case-1	1.2 million
Case-2	2.5 million
Case-3	4.1 million

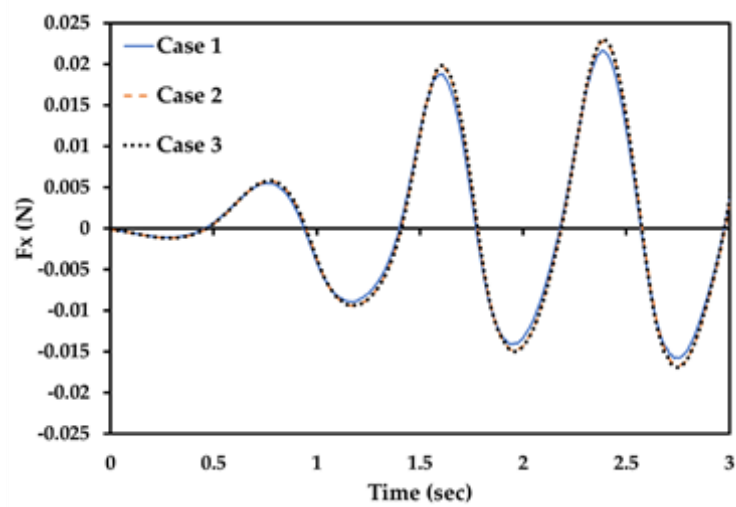


Figure 6.9 – Force on fixed hydrofoil in x-direction

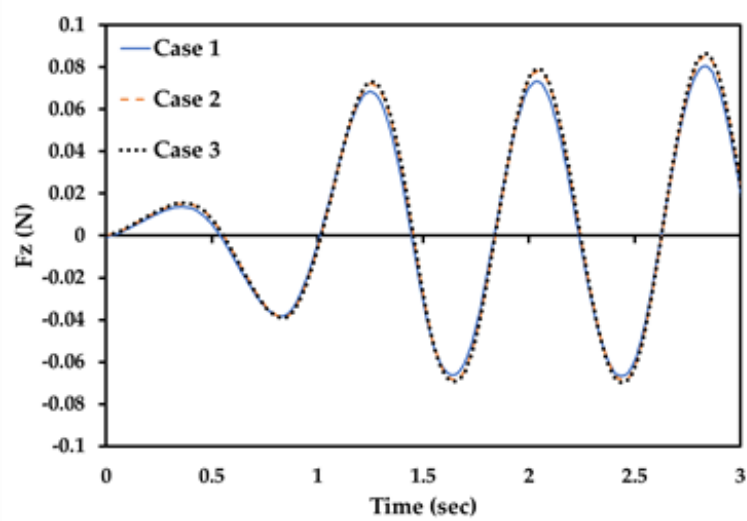
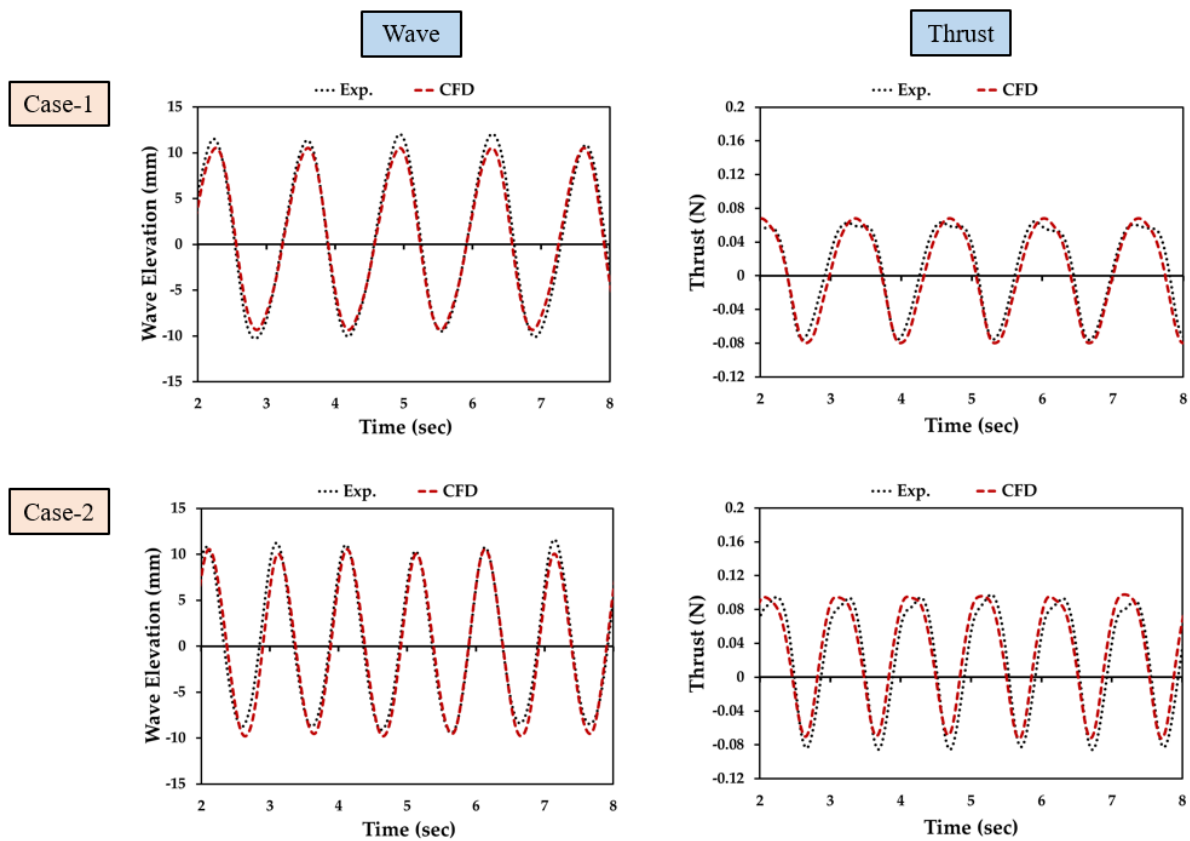


Figure 6.10 – Forces on fixed hydrofoil in z-direction

Results in Figure 6.9 and Figure 6.10 show that case 1 is slightly underestimating the peak value. However, case 2 and case 3 show a good agreement therefore, case 2 mesh resolution was selected for the 2-way FSI simulation to save the computation time.

6.4.2 Results comparison

The thrust forces generated by a passive flapping foil were measured experimentally in various waves and elastic conditions and reported in chapter 2. A CFD simulation of passive flapping foil in waves was compared with the experimentally recorded time series data. Figure 6.11 shows the comparison of wave and thrust profiles from 2 to 8 seconds for four load cases displayed in Table 6.1. The comparison of results validates the numerical method qualitatively also quantitatively.



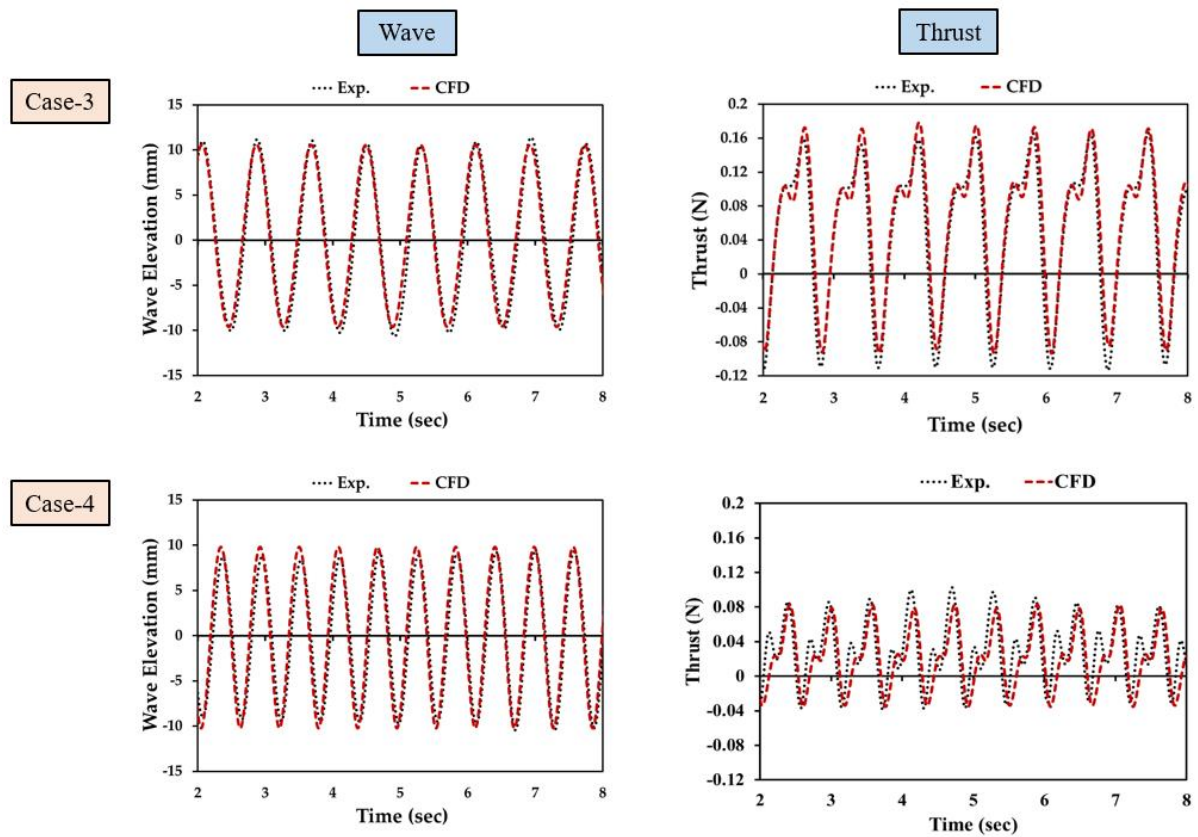


Figure 6.11 – Comparison of wave elevation and thrust forces

6.5 Conclusion

In this study, 2-way FSI with CFD simulation was used to evaluate the thrust forces generated by a passive flapping foil in regular waves. Simulation results confirm the generation of thrust forces due to the flapping motion of foil in passive mode. Foils were flapping at a set location and generating thrust forces against the direction of incoming waves, which was vital for the design of stationkeeping system of a floater in waves.

Chapter 7 Active Flapping Foil

The purpose of this study was to investigate the possibilities of using flapping foils for designing a stationkeeping system of a floater in short waves. In order to do that, the evaluation and comparison of thrust forces of each foil in active and passive modes are necessary. Therefore, in this study, a flapping foil was set to oscillate at a fixed location and the thrust forces were evaluated for the active mode of flapping foil in still water and short waves for five flapping frequencies. Also, the CFD model was validated by comparing the thrust forces generated by fixed foil and passive flapping foil. This work was reported in [37].

7.1 Forced oscillation

The forced flapping frequencies are generated by an electric motor that creates a rotational motion and a lever connected to it converts the rotational motion into linear vertical motion which drives the trailing edge of the flapping hydrofoil. The active mode flapping frequencies can be adjusted by adjusting the rpm of the motor.

Table 7.1 – Mesh resolution

Load Cases	Flapping frequency (Hz)	Flapping period (sec)
Flap-1	0.71	1.4
Flap-2	0.83	1.2
Flap-3	1.0	1.0
Flap-4	1.18	0.85
Flap-5	1.33	0.75

In this section, CFD numerical tool was used to evaluate the thrust forces generated by the five flapping frequencies of the motor as displayed in the Table 7.1. In active mode of flapping foil, trailing edge of the hydrofoil was displaced forcibly with five different frequencies as shown in the Figure 7.1.

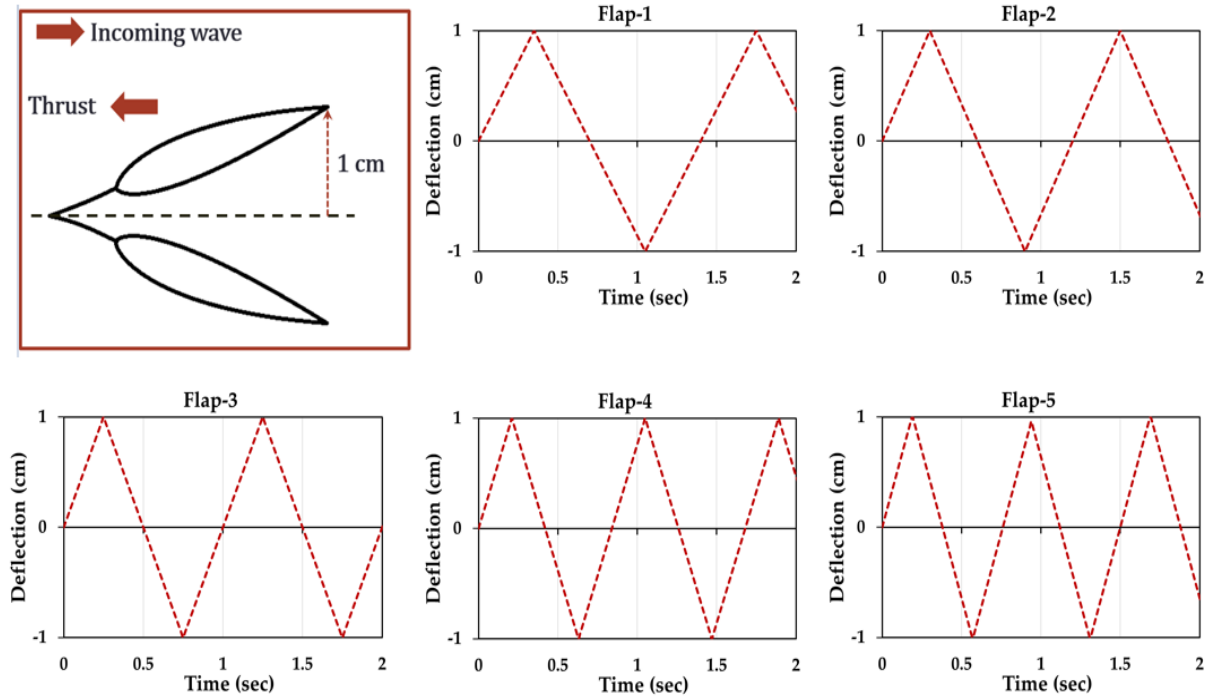


Figure 7.1 – Forced flapping profile

7.2 Fixed hydrofoil

For the incident short wave displayed in Table 7.2, an experiment was carried out for a fixed foil to capture the thrust forces measured in x-direction as shown in Figure 7.2, therefore, 1 mm thick HDPE elastic plate was replaced by a rigid stainless steel plate of same thickness and sinusoidal variation of force in the surge (F_x) was recorded and compared with the numerically evaluated results using CFD.

Table 7.2 – Wave specification

Wave	Wavelength (m)	Wave height (m)
Short wave	0.52	0.02

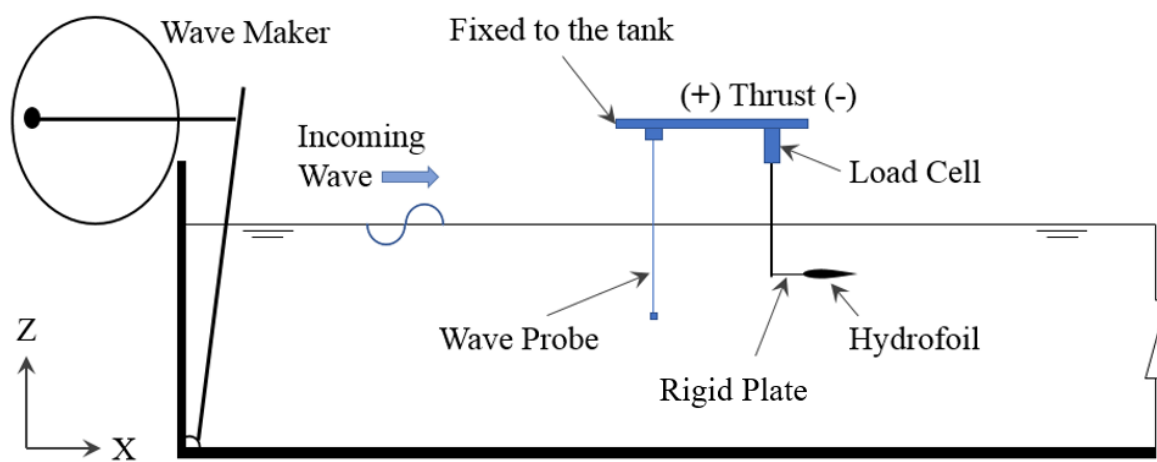
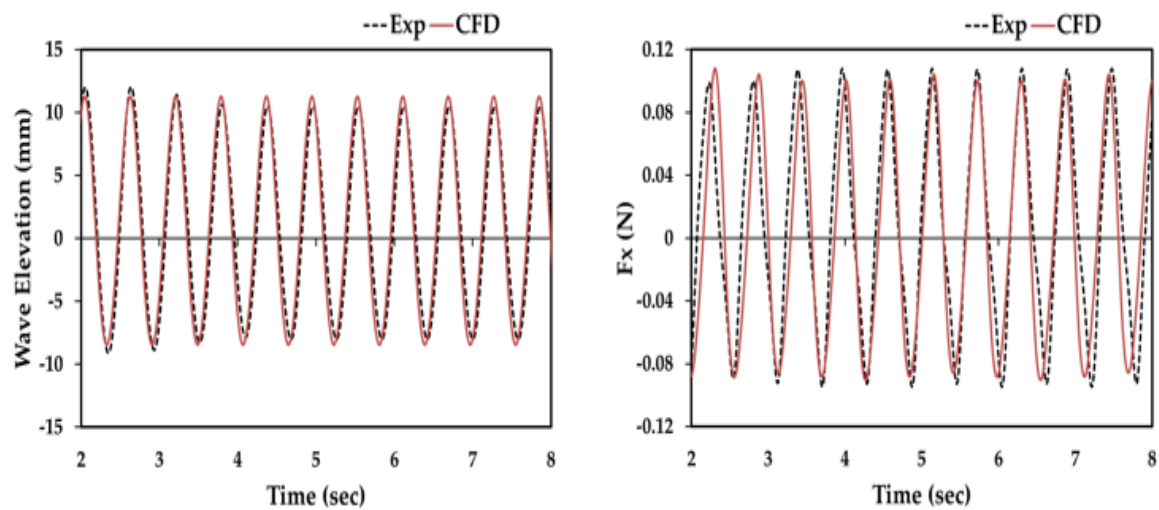
Figure 7.2 – Experimental setup to measure F_x for a fixed hydrofoil in short waves.

Figure 7.3 – Comparison of wave profile and force in x-direction

Figure 7.3 shows the comparison of wave elevations and the pressure force variations on the fixed foil in time domain respectively. The CFD numerical results were in good agreement with experimental data.

7.3 Flapping in still water

Thrust forces generated by the active flapping foil in still water with five flapping frequencies were evaluated using CFD-FSI simulation. Figure 7.4 (a), (b), (c), (d) and (e) show the thrust plots with the trailing edge deflection of the hydrofoil for flap-1, flap-2, flap-3, flap-4 and flap-5 respectively.

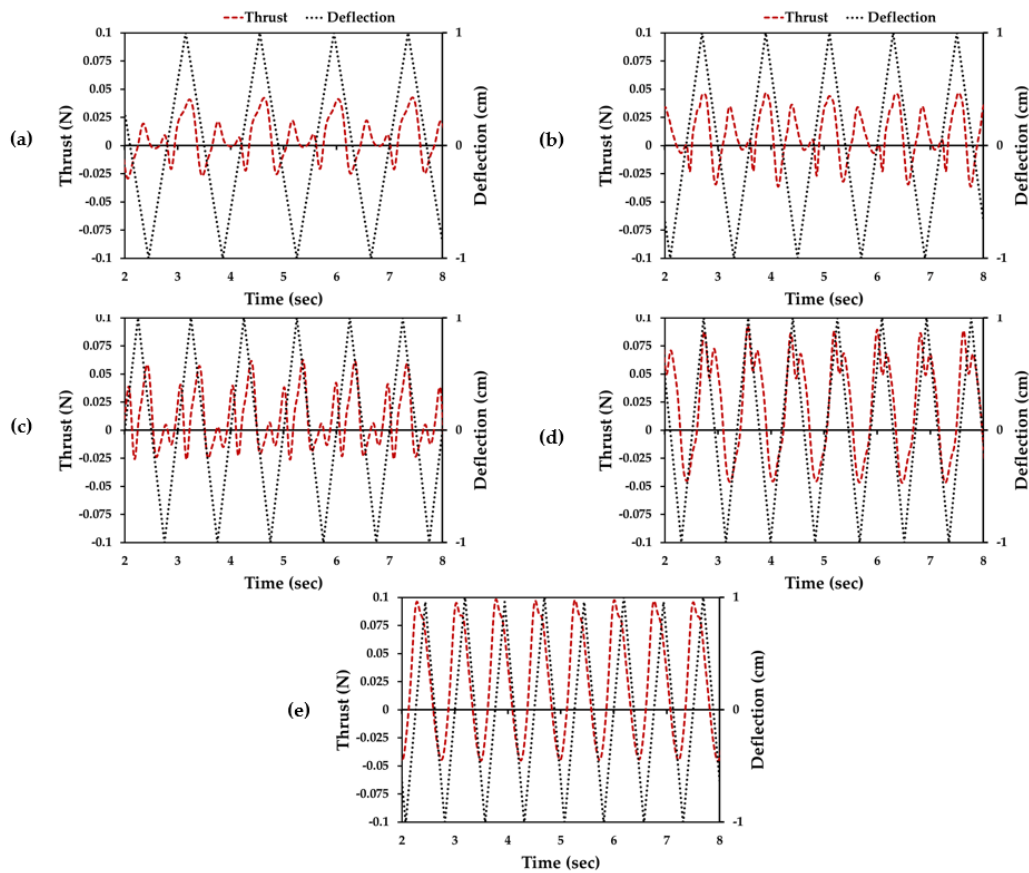


Figure 7.4 – Thrust plot in still water using CFD (a) Flap-1; (b) Flap-2; (c) Flap-3; (d) Flap-4; (e) Flap-5

Results prove that the thrust forces can be generated by the active flapping motion of the foil in still water. As the flapping frequency increased, the magnitude of thrust forces increased, however, the number of thrust peaks decreased.

7.4 Active mode results in short waves

Finally, five active modes of flapping foil were simulated in a short wave using 2-way FSI simulation and the results are displayed in Figure 7.5 (b), (c), (d), (e) and (f) for flap-1, flap-2, flap-3, flap-4, and flap-5 respectively.

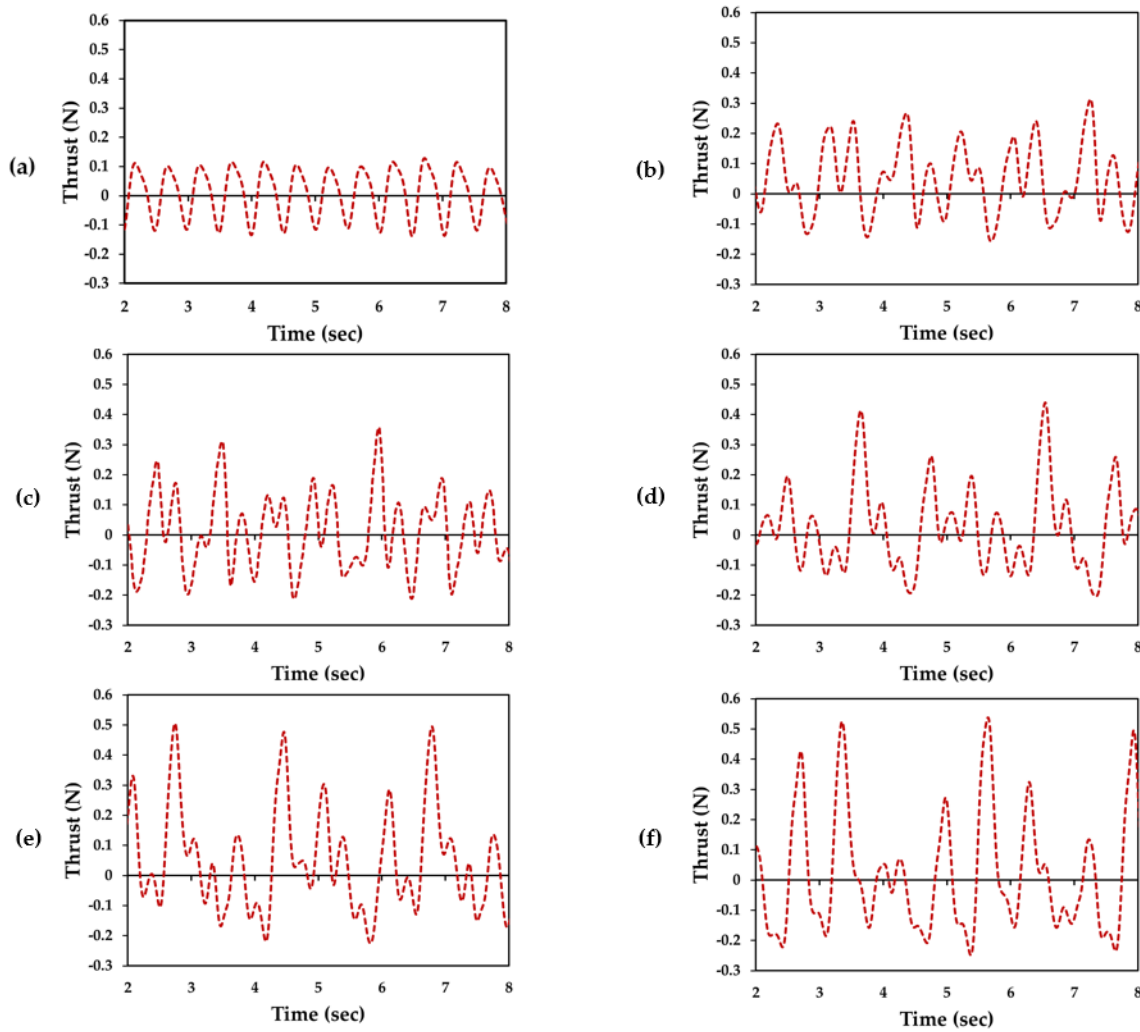


Figure 7.5 –Thrust plot in short waves (a) Passive flapping foil (Experiment); (b) Flap-1 (CFD); (c) Flap-2 (CFD); (d) Flap-3 (CFD); (e) Flap-4 (CFD); (f) Flap-5 (CFD)

Results show that the magnitude of thrust forces increased drastically in active mode with waves compared to active mode in still water and fixed hydrofoil in waves, due to its ability to convert wave energy into propulsive energy, a fixed foil couldn't create an effective angle of attack to efficiently transform the wave energy into propulsive energy and in still water condition, there was a no incoming wave or fluid flow to generate lift and thrust forces for the angle of attacks created by the active flapping. However, 2-way FSI analysis could couple the effects of waves with active flapping, therefore, higher thrust peaks are evaluated.

Figure 7.5 (a) shows the experimentally measured thrust data of passive flapping foil in a short wave specified in Table 7.2. In the passive mode, there was no significant difference in the positive and negative thrust peaks, hence it wasn't enough to prevent the floater from drifting during the stationkeeping tests [38]. Conversely, Active modes are dominating in the positive side of the thrust plots. Therefore, active flapping foil could be a potential solution for the stationkeeping problems in the short waves.

7.5 Conclusion

In this study, 2-way FSI with CFD simulation was used to evaluate the thrust forces generated by the active flapping foils in a short wave and still water conditions. Simulation results confirm the generation of thrust forces due to the flapping motion of foil in both active modes. Foils were flapping at a set location and generating thrust forces against the direction of incoming waves, which was vital for the design of the stationkeeping system of a floater in waves.

Results prove that the active flapping can generate thrust forces for the stationkeeping of a floater in short waves. And the magnitude of thrust forces can be controlled by adjusting the flapping frequency of the foil. And for further development of the flapping foil stationkeeping system, CFD can be a very efficient tool to evaluate the dynamic behaviour of it.

In the future, an experiment of the stationkeeping model with active flapping foils in short waves should be performed.

Chapter 8 Validation of Results

This chapter makes a comparison of three methods discussed in previous chapters to evaluate thrust forces generated by a flapping foil in waves. First method was experimental, where a loadcell was used to measure the thrust forces in time domain for a hydrofoil flapping at a set location. The experiments were carried out in a wave flume of 35 m long, 0.5 m wide and 0.6 m deep. The water level was at 0.4 m during experiments and foil was submerged 5 cm from the free surface. The second method was empirical formula that was developed from the experimental results. More than 200 experiments carried out to generate enough data for deriving an empirical formula for thrust forces of passively flapping hydrofoil using multiple regression analysis. Third method was a CFD numerical method, where multiphase 2-way FSI problem was simulated to evaluate thrust forces in time domain. Finally, a comparison of all the three methods are displayed and discussed in this chapter.

8.1 Results comparison

Table 8.1 – Load cases for CFD simulation

Load case	λ (m)	T (s)	ω (rad/s)
1	0.52	0.58	10.86
2	1.01	0.81	7.75
3	1.49	1.01	6.22
4	2.30	1.36	4.63

For making a comparison of three methods to estimate thrust forces of a flapping foil that validates each other, four load cases were selected as displayed in Table 9.1.

Since, experimentally recorded data can be compared in time domain with numerically obtained CFD results, but empirical formula can only estimate the mean thrust of the flapping foil, therefore, mean of the experimental and numerical results are obtained as shown in Figure 9.1.

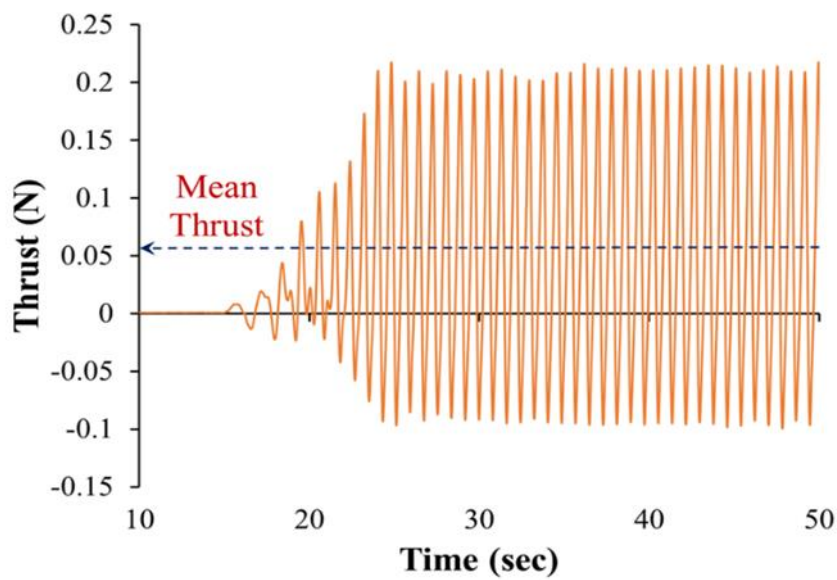


Figure 8.1 – Estimation of mean thrust

Finally, thrust coefficient was evaluated for comparison using following formula;

$$C_T = \frac{T}{\frac{1}{2} \rho (A_F) V^2}$$

Where;

T = Mean thrust force (N)

ρ = 1000 kg/m³

A_F = Area of foil (m²)

V = $C\Omega$ A (m/s²)

ω = Wave frequency (rad/s)

A = Wave amplitude (m)

Thrust coefficient (C_T) from the empirical formula was estimated as follows;

$$\begin{aligned} \ln(C_T^2) = & -7.13 + 191.36 \times F_n - 1.57 \times \ln(E_p) - 1.02 \times A_d - 6.55 \times A_r - 636 \times W_s + 2422 \times (W_s)^2 \\ & - 100.2 \times F_n \times A_r + 1.51 \times \ln(E_p) \times A_r + 193.16 \times A_r \times W_s \end{aligned}$$

Table 8.2 – Estimation of thrust coefficient from empirical formula

-7.13	191.36×Fn	1.57×Ln(Ep)	1.02×Ad	6.55×Ar	636×Ws	2422×(Ws)2
-7.13	29.6730	-5.8071	-1.043E-08	-0.9825	-24.462	3.5828
-7.13	23.6749	-6.8665	-1.047E-08	-0.9825	-12.594	0.9497
-7.13	25.3387	-7.5565	-1.041E-08	-0.9825	-8.537	0.4364
-7.13	23.4917	-8.4840	-1.038E-08	-0.9825	-5.530	0.1831

- 100.2×Fn×Ar	1.51×Ln(Ep)×Ar	193.16×Ar×Ws	Ln(ct^2)	Ct
-2.3306	0.8378	1.1144	-5.50	0.064
-1.8595	0.9906	0.5737	-3.24	0.198
-1.9902	1.0902	0.3889	1.06	1.697
-1.8451	1.2240	0.2519	1.18	1.803

Table 9.1 shows the calculation done for estimating the thrust coefficients of the flapping foil for load cases shown in Table 9.1, Table 9.2 displays the thrust coefficients of experimental

and numerical methods. Figure 9.2 shows the comparison of all three methods discussed in the previous chapters.

Table 8.3 – Thrust coefficient of experimental and numerical methods

	Experiment		Numerical	
λ (m)	T(N)	Ct	T(N)	Ct
0.52	-0.0058	-0.0611	-0.0073	-0.0772
1.01	0.0122	0.2537	0.0059	0.1235
1.49	0.0442	1.4281	0.0370	1.1954
2.30	0.0301	1.7524	0.0318	1.8532

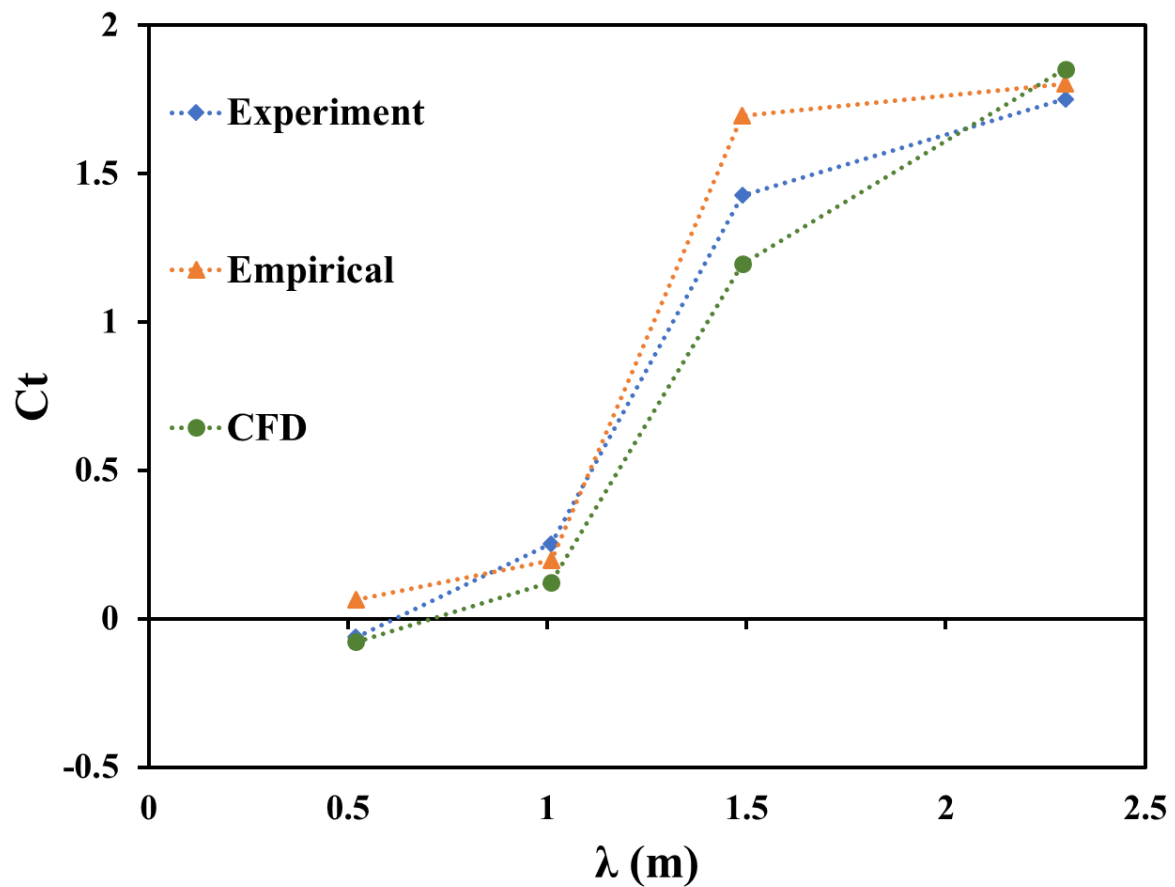


Figure 8.2 – Comparison of results

8.2 Discussion

Flapping hydrofoil oscillates near the free surface using wave energy and highly dynamic in nature, therefore, no method can be trusted for the estimation of dynamic forces without validation by the alternative means. Figure 9.2 shows the comparison of thrust coefficients of a flapping foil evaluated from three different methods and results confirmed that all the three methods follow the same trend and qualitatively validates each other. It also validates the method used to derive the empirical formula.

Chapter 9 Conclusion and Future Work

This chapter includes the summary of conclusions from all the above chapters and future of the present study.

9.1 Conclusions

This study was customized for the marine applications of flapping foils and flapping plates to the stationkeeping in waves. Neither the hydrofoil nor a flap system is anything new, but it's the combination and application. A combination of elastic plate and rigid foil assured a smooth flapping also minimized the complexity in flapping by eliminating the phase lag between heave and pitch motions of hydrofoil. The addition of elastic plate made the flapping similar to the first mode oscillation of a cantilever plate, fixed at one end and free at other. This model can generate variety of thrust forces without changing the hydrofoil, a change in elastic plate can produce the desired thrust force. Since, thrust forces can be generated by the flapping foil at a set location using incoming wave energy, stationkeeping design can be viable using it. Therefore, the thrust generating abilities of the new flapping model was investigated experimentally, the methods are discussed in chapter 2. Results were pragmatic and it confirmed the dependency of thrust extent on the elasticity of plate and wave profile. In addition, an empirical formula to evaluate mean thrust force of passive flapping foil in waves was developed using dimensional and regression analysis, reported in chapter 3. Further, a combination of flapping foils was investigated because generation of thrust forces could drift the floater against the wave propagation that is not the objective of stationkeeping model. Therefore, combination of foils was examined to attain stationkeeping goals. Results confirmed that stationkeeping can be made possible by incorporating azimuth control or by adjusting the elastic plates, described in chapter 4. Also, experiments were carried out by replacing the hydrofoil with a flat plate to further simplify the model, because thrust produced by the flapping plate was sufficient to meet the stationkeeping requirements and stationkeeping model with flapping plates performed better in keeping position compared to flapping foils. Therefore,

similar investigations were executed for a flapping flat plate and an empirical formula was derived for the thrust estimation in chapter 5.

Due to technical advancements in the field of computational fluid dynamics (CFD), computational structural mechanics (CSM) and coupling of both have made the numerical analysis more realistic to perform. Therefore, 2- way fluid structure interaction (FSI) simulation was performed using ANSYS Workbench 19.2 to validate the results obtained from the experiments. Results reported in chapter 8 validated the use of empirical formula to predict mean thrust forces of a passive flapping foil. Further, active mode of flapping foil was simulated using CFD because experimentally, thrust measurement in active mode is complicated. Also, active mode could generate additional thrust forces when passive mode wasn't effective such as short waves.

Therefore, the study suggests that a design of stationkeeping model using flapping foils are possible by developing a control system which can utilize active mode, passive mode and azimuth angle.

9.2 Future works

In future, a stationkeeping system can be developed that can be installed regardless of any water depth, can be relocated and cost saving as well. Study made in this thesis would be useful to design a control system and a prototype stationkeeping model can be experimented in the lab facility and open sea conditions. Also, the empirical formula should be modified by including the effects of azimuth angles.

References

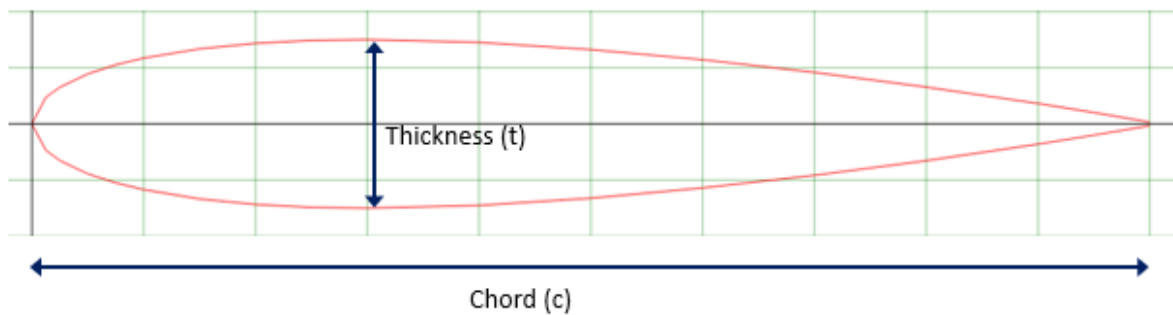
- [1] Hermann Linden, “Improved combination with floating bodies, of fins adapted to effect their propulsion. GB Patent 14,630. Filed Aug. 1, 1895. Patented Jul. 18, 1896.,” GBD189514630 (A).
- [2] O. Schulze, “Wave motor,” 1033476, 1911.
- [3] P. Science, “Wave power runs model boat,” *Pop. Sci.*, no. April, 1935, p. 26, 1935.
- [4] J. S. McCubbin, “Wave serve as boat’s engine,” *Pop. Sci.*, no. Feb, 1950, p. 224, 1950.
- [5] J. A. Gause, “Flexible fin propulsion member and vessels incorporated same.,” 1176559, 1966.
- [6] Y. Terao and H. Isshiki, “Wave devouring propulsion sea trial,” in *Eighteenth symposium on Naval Hydrodynamics*, 1991, pp. 287–296.
- [7] O. Fabre, “Japan sailor takes on pacific in wave-powered boat,” *Reuters*, 2008.
- [8] J. M. K. G. Kazi Shah Nawaz Ripon, “Optimizing Bio-Inspired Propulsion System Using Genetic Algorithm,” in *Computational Intelligence (SSCI), 2017 IEEE Symposium Series on*.
- [9] E. Yu, J.; Tan, M.; Wang, S.; Chen, “Development of a biomimetic robotic fish and its control algorithm,” *IEEE Trans. Syst. Man Cybern*, vol. 34, pp. 1789–1810, 2004.
- [10] F. E. Fish, “Advantages of Natural Propulsive Systems.,” *Mar. Technol. Soc. J.*, vol. 47, pp. 37–44, 2013.
- [11] S. Bøckmann, E.; Steen, “Experiments with actively pitch-controlled and spring-loaded oscillating foils.,” *Appl. Ocean Res.*, vol. 48, pp. 227–235, 2014.
- [12] K. A. Filippas, E.S.; Belibassakis, “Hydrodynamic analysis of flapping-foil thrusters operating beneath the free surface and in waves,” *Eng. Anal. Bound. Elem.*, vol. 40, pp.

- 47–59, 2014.
- [13] D. A. Read, F. S. Hover, and M. S. Triantafyllou, “Forces on oscillating foils for propulsion and maneuvering,” *J. Fluids Struct.*, vol. 17, no. 1, pp. 163–183, 2003.
- [14] F. S. Hover, Haugsdal, and M. S. Triantafyllou, “Effect of angle of attack profiles in flapping foil propulsion,” *J. Fluids Struct.*, 2004.
- [15] Ulysses S. Harkson; San Mateo;, “WATER CRAFT HAVING HYDROPLANES, 2,821,948 United States Patent Office, Claim. (CI. 114-66.5),” 1958.
- [16] S. F. Evangelos, “Augmenting ship propulsion in waves using flapping foils initially designed for roll stabilization,” in *YSC 2015. 4th International Young Scientists Conference on Computational Science*, 2015, pp. 103–111.
- [17] Y. S. Peng Liu, Yebao Liu, Shuling Huang, Jianfeng Zhao, “Effects of Regular Waves on Propulsion Performance of Flexible Flapping Foil,” *Appl. Sci.*, vol. 8, p. 934, 2018.
- [18] P. Prempraneerach, F. S. Hover, and M. S. Triantafyllou, “The effect of chordwise flexibility on the thrust and efficiency of a flapping foil,” *Int. Symp. Unmanned Untethered Submers. Technol.*, 2003.
- [19] W. Zhou, K.; Liu, J.; Chen, “Study on the Hydrodynamic Performance of Typical Underwater Bionic Foils with Spanwise Flexibility.,” *Appl. Sci.*, vol. 7, p. 1120, 2017.
- [20] Z. Liu, F. B. Tian, J. Young, and J. C. S. Lai, “Flapping foil power generator performance enhanced with a spring-connected tail,” *Phys. Fluids*, vol. 29, no. 12, 2017.
- [21] G. D. Xu, W. Y. Duan, and B. Z. Zhou, “Propulsion of an active flapping foil in heading waves of deep water,” *Eng. Anal. Bound. Elem.*, vol. 84, pp. 63–76, 2017.
- [22] and L. G. Paolo Blondeaux, Francesco Fornarelli, “Numerical experiments on flapping foils mimicking fish-like locomotion,” *Phys. Fluids*, vol. 17, 2005.
- [23] Y.-H. Xie, W. Jiang, K. Lü, and D. Zhang, “Review on research of flapping foil for power generation from flow energy,” *Zhongguo Dianji Gongcheng*

-
- Xuebao/Proceedings Chinese Soc. Electr. Eng.*, vol. 36, no. 20, pp. 5564–5575, 2016.
- [24] K. A. Belibassakis, E. S. Filippas, J. Touboul, and V. Rey, “Hydrodynamic analysis of oscillating hydrofoils in waves and currents,” in *Towards Green Marine Technology and Transport*, 2015, pp. 185–192.
- [25] H. Silva, L.W.A.D.; Yamaguchi, “Numerical study on active wave devouring propulsion,” *J. Mar. Sci. Technol.*, vol. 17, pp. 261–275, 2012.
- [26] A. Nematbakhsh, E. E. Bachynski, Z. Gao, and T. Moan, “Comparison of wave load effects on a TLP wind turbine by using computational fluid dynamics and potential flow theory approaches,” *Appl. Ocean Res.*, 2015.
- [27] H. Bredmose and N. G. Jacobsen, “Breaking Wave Impacts on Offshore Wind Turbine Foundations: Focused Wave Groups and CFD,” 2011.
- [28] J. Westphalen, “Extreme Wave Loading on Offshore Wave Energy Devices using CFD,” 2011.
- [29] B. Blocken, T. Defraeye, E. Koninckx, J. Carmeliet, and P. Hespel, “CFD simulations of the aerodynamic drag of two drafting cyclists,” *Comput. Fluids*, 2013.
- [30] A. Jameson, “Optimum aerodynamic design using CFD and control theory,” 1995.
- [31] B. K. Lee, “Computational fluid dynamics in cardiovascular disease,” *Korean Circulation Journal*. 2011.
- [32] Z. Sun and L. Xu, “Computational fluid dynamics in coronary artery disease,” *Comput. Med. Imaging Graph.*, 2014.
- [33] J. Lee, Y. J. Park, K. J. Cho, D. Kim, and H. Y. Kim, “Hydrodynamic advantages of a low aspect-ratio flapping foil,” *J. Fluids Struct.*, vol. 71, pp. 70–77, 2017.
- [34] R. Kumar and H. Shin, “Thrust estimation of a flapping foil attached to an elastic plate using multiple regression analysis,” *Int. J. Nav. Archit. Ocean Eng.*, 2019.
- [35] J. M. Kane, “ANSYS FLUENT 12.0 User’ Guide,” *Acta Psychiatr. Scand.*, 2011.

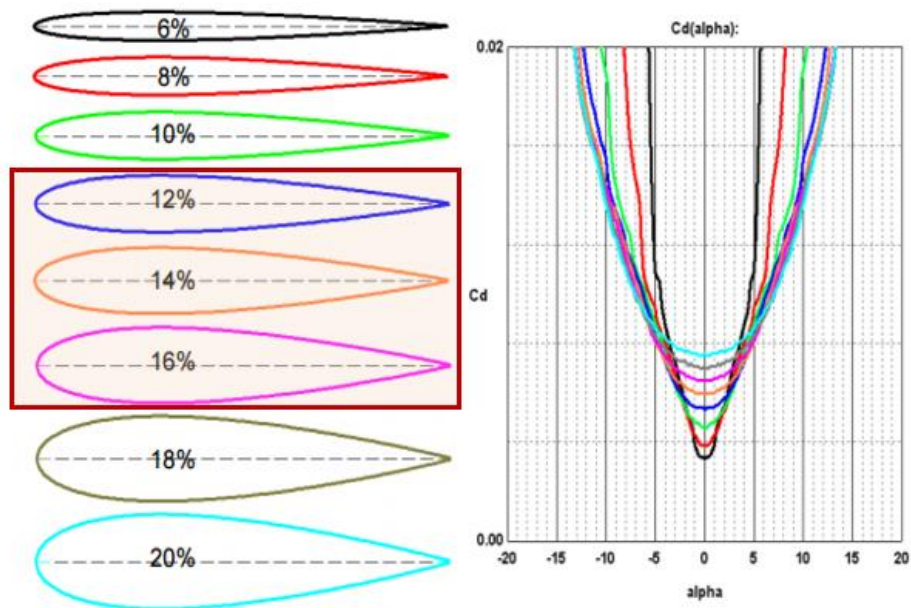
-
- [36] J. A. N. Hengstler, “Influence of the fluid-strudture interaction on the vibrations of structures Doctoral thesis,” ETH Zurich, 2013.
 - [37] R. Kumar and H. Shin, “Thrust Prediction of an Active Flapping Foil in Waves Using CFD,” *J. Mar. Sci. Eng.*, vol. 7, no. 11, 2019.
 - [38] S. H. Sim Woolim, Kumar Rupesh, Yu Youngjae, Kim Junbae, Seo Beongcheon, “Experimental study of the stationkeeping system of a floater using flapping foils in waves,” in *8th PAAMES and AMEC*, 2018, pp. 359–362.

Appendix A Foil Design

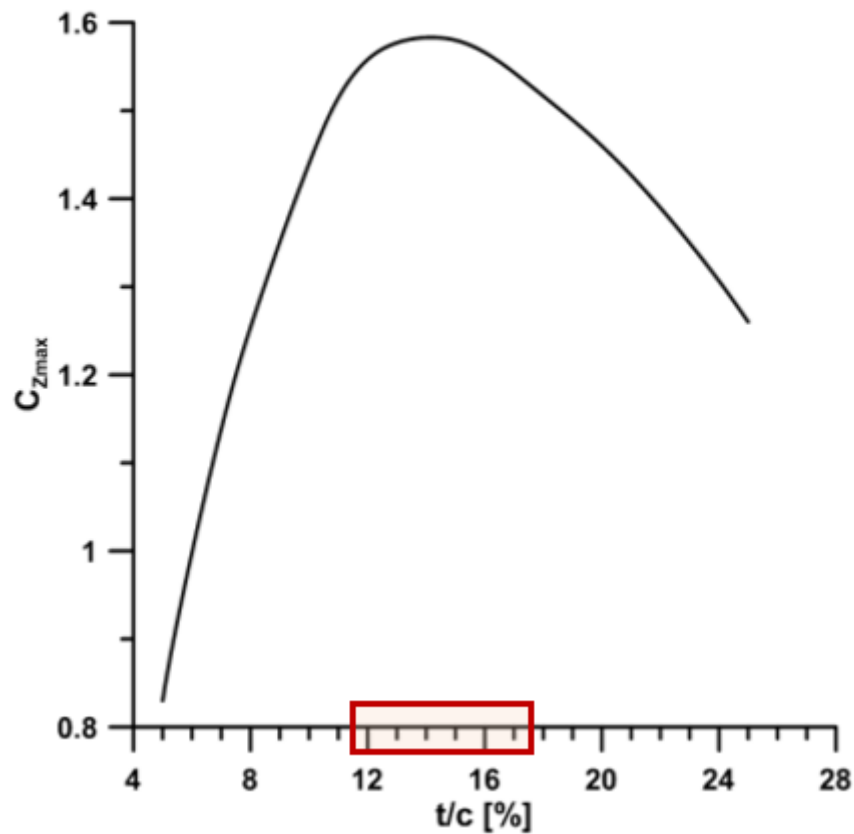


A.1 Lift and drag coefficients

Effect of airfoil thickness on drag coefficient



Effect of airfoil thickness on lift coefficient



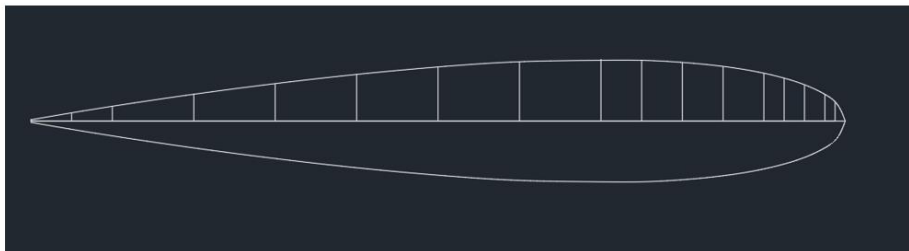
[Ref: https://itlims-zsis.meil.pw.edu.pl/pomoce/BIPOL/BIPOL_1_handout_8A.pdf]

Section 12 to 16 have higher lift coefficient and lower drag coefficient.

Therefore, NACA0015 section was selected.

Final Design

- Foil = **NACA_0015**
- Span = 20cm
- Chord = 8cm
- Max. Thickness 15% at 30% Chord.
- Camber = 0



NACA 0015	
1.0000	0.00158
0.9500	0.01008
0.9000	0.01810
0.8000	0.03279
0.7000	0.04580
0.6000	0.05704
0.5000	0.06617
0.4000	0.07254
0.3000	0.07502
0.2500	0.07427
0.2000	0.07172
0.1500	0.06682
0.1000	0.05853
0.0750	0.05250
0.0500	0.04443
0.0250	0.03268
0.0125	0.02367
0.0000	0.00000